UNIVERSITÄTSKLINIKUM HAMBURG-EPPENDORF

Zentrum für Diagnostik

Prof. Dr. rer. nat. Stefan Linder

"Uptake of *Candida albicans* and *Candida auris* by primary macrophages is mediated by phagocytic podosomes"

Dissertation

zur Erlangung des Doktorgrades der Medizin
an der Medizinischen Fakultät der Universität Hamburg

eingereicht von:

Rawan Batlouni
Aus dem Libanon

Hamburg 2024

Annahmevermerk:

Angenommen von der

Medizinischen Fakultät der Universität Hamburg am 07.03.2025

Veröffentlicht mit Genehmigung der

Medizinischen Fakultät der Universität Hamburg.

Prüfungsausschuss, Vorsitzender: Prof. Dr. Pablo J. Sáez

Prüfungsausschuss, Zweitgutachter: Prof. Dr. Stefan Linder

Table of contents

Acceptance note……i

Table of contents…… ii

1. Introduction……1

1.1 Phagocytosis as a cellular process……1

1.2 Actin rearrangements during phagocytosis……2

1.3. Matrix associated podosomes……3

1.4 Phagocytic podosomes……5

1.5 Monocytes and macrophages, different phenotypes……5

1.5.1 M1 macrophages……6

1.6 *Candida species*……7

1.6.1 *Candida albicans*……7

1.6.2 *Candida auris*……8

1.7 Working hypothesis/ research question……9

2. Materials and methods……11

2.1. Materials……11

2.1.1. Devices……11

2.1.2. Microscopes……12

2.1.3. Software……17

2.1.4 Consumables……17

2.2. Methods……22

2.2.1 General……23

2.2.2 Monocytes/macrophages……23

2.2.3 Candida……25

2.2.4 Infection of macrophages with Candida species……25

2.2.5. Fluorescent staining ……26

2.2.6 Immune-fluorescent staining……27

2.2.8 Live cell imaging……27

2.2.9 Chemical/pharmacological inhibition of cellular proteins……28

3. Results……29

3.1 Actin Foci on Candida phagosome……29

3.2 Identification of main protein composition of podosome-like structures……29

3.3 Tracking podosome-like structures on Candida phagosomes……32

3.4 Overexpression of MT1-MMP with lifeact construct in primary macrophages……35

3.5 Inhibition of tyrosine kinase by PP2……37

4. Discussion……42

4.1 Identification of phagocytic podosomes on Candida phagosomes……42

4.2 Similarity in protein composition of matrix and phagocytic podosomes……42

4.3 phagocytic podosomes' lifespan and density analysis……44

4.4. Association of phagocytic podosomes with degradation enzymes……45

4.5. Susceptibility of phagocytic podosomes to chemical inhibition……49

4.6. Conclusion……48

5. Summary……50

6. List of abbreviations……51

7. Bibliography-literature review……54

8. Acknowledgement……59

9. Curriculum vitae……60

10. Statutory declaration……62

1-Introduction

This introduction is dedicated to providing a general overview about phagocytosis as a cellular process in primary macrophages, especially that these macrophages are known to express matrix associated podosomes as constitutive structures. It further provides background information about the differentiation of monocytes to macrophages and the involvement of Podosomes and actin rearrangements in the process of phagocytosis of Candida species. Throughout this introduction, relevant research methodologies and methodological backgrounds will be discussed as well.

1.1 Phagocytosis as a cellular process

Phagocytosis is a vital process for nutrition in unicellular organisms, however in multicellular organisms this function is performed by specialized cells called phagocytes. In brief, Phagocytosis involves recognizing and engulfing particles larger than 0.5 µm, forming a phagosome—a vesicle derived from the plasma membrane (Rosales & Uribe-Querol - BioMed Research International – 2017).

Among phagocytic cells, we distinguish professional phagocytes on one hand such as monocytes, macrophages, neutrophils, dendritic cells, osteoclasts, and eosinophils, which are responsible for eliminating microorganisms and presenting them to cells of the adaptive immune system. On the other hand, there exist nonprofessional phagocytes like fibroblasts, epithelial cells, and endothelial cells that can still participate in phagocytosis, despite being less efficient in ingesting microorganisms, but they still play a critical role in eliminating apoptotic bodies. (Rosales & Uribe-Querol - BioMed Research International – 2017).

The initial stage of phagocytosis involves identification of the targeted particle for ingestion which is facilitated by specialized receptors on the cell membrane. This detection process is governed by means of binding of opsonins, or pathogen-associated molecular patterns (PAMPs) of the foreign particle to Toll-like receptors (TLRs) and specific G-protein coupled receptors on the cell surface that contribute to priming the cell for phagocytosis (Uribe-Querol & Rosales - Frontiers in Immunology – 2020). This process then continues through the initiation of the internalization process, that develops into the creation of a specialized vacuole named a

phagosome that will further undergo a maturation process until it transforms into a phagolysosome (Uribe-Querol & Rosales - Frontiers in Immunology – 2020).

Knowing that The process of uptaking large particulate materials necessitates a substantial reconfiguration of cell morphology around the designated target in a controlled manner that is constrained by biophysical limitations, Experimental and theoretical studies have identified critical facets related to the interconnected biophysical properties of receptors, membranes, and the actin cytoskeleton that contribute to determining the success of internalizing large particles and the entire process of phagocytosis.(Jaumouillé & Waterman - Frontiers in Immunology – 2020)

This cytoskeletal rearrangement that is deployed in phagocytosis is found to be governed by mechanistically distinct processes, one of these described as the zipper mechanism, has been demonstrated to mediate phagocytosis across multiple cell and receptor types and for a wide range of target particles where sequential engagement of cell surface receptors to ligands on the target particle lead to a complete wrapping of the particle by the plasma membrane. (Jaumouillé & Waterman - Frontiers in Immunology – 2020).

The best-studied pathways in mammalian professional phagocytosis are Fc-mediated phagocytosis, which involves binding of Immunoglobulin g (IgG) to Fc γ receptors (FcγR), and complement-mediated phagocytosis, which involves binding of the complement molecule iC3b to αMβ2 or αXβ2 integrins, also named complement receptors (CR) 3 and 4, respectively (Jaumouillé & Waterman - Frontiers in Immunology – 2020).

1.2 Actin rearrangements during phagocytosis

Phagocytosis relies on five key physical factors: receptors on the cell surface attaching to ligands on the target, generating enough force to overcome cortical tension and start forming the phagocytic cup, extending the cup along the particle's surface, having sufficient membrane area, and completing membrane fission to enclose and absorb the target (Jaumouillé & Waterman, Frontiers in Immunology, 2020).These constraints are all dependent on the actin cytoskeleton organization at the front of a migrating cell and at the phagocytic cup. This

involves the formation of a branched network of actin filaments which is mediated by the Arp2/3 complex and activated at the plasma membrane by an NPF (nucleation-promoting factor) recruited by an active Rho GTPase. Actin dynamics are regulated by capping proteins, elongation factors, disbranching, severing, and monomer binding proteins. Formation of linear actin structures, such as the stress fibers and transverse arcs at the lamella involve the bundling proteins α-Actinin and Fascin, as well as actin nucleation by formins and Myosin II mini-filaments. These actin structures are stabilized on the substratum by adhesions. At the phagocytic cup, adhesions are mediated by Fcγ receptors, β2 integrins or other phagocytic receptors(Jaumouillé & Waterman - Frontiers in Immunology – 2020).

1.3. Matrix associated podosomes

Podosomes are micron-sized structures that are formed at the interface between an adhering cell and the substratum (Linder and Aepfelbacher, 2003). They were first described in Rous sarcoma virus transformed fibroblasts as adhesion structures that resembled cell feet (Tarone et al., 1985). They were later studied as dynamic F-actin-based adhesion spots associated with motile cells of the myeloid and nonmyeloid lineage (Schachtner et al. - Cytoskeleton – 2013). These podosomes are typically formed in cells of the monocytic lineage such as macrophages (Linder et al., 1999), immature dendritic cells (Burns et al., 2001), and osteoclasts (Destaing et al., 2003). However, podosomes can also be formed by endothelial cells (Moreau et al.,2003), neural crest cells (Murphy et al., 2011), or smooth muscle cells stimulated with phorbol ester (Burgstaller and Gimona, 2005).

These podosomes carry crucial roles in facilitating cell motility especially through their expression on leading cell edge protrusions, furthermore they are also associated with enabling the cells mechanosensing properties in which they sense the ECM. Podosomes can also carry out degradative functions through their protease activity in which they remodel and degrade extracellular environments (Schachtner et al. - Cytoskeleton – 2013). Additionally these

podosomes are found to be dynamic centers of signaling where they can form interconnected networks in many cell types, and often show superstructures indicating a higher organization and interpodosome communication/signaling within cells that may allow them to function as a large unit rather than as individual spots. Examples of these podosome superstructures are evenly distributed podosomes during spreading ,clusters, rings, belts of podosomes, or podosomal rosettes in specific adhesive events. (Schachtner et al. - Cytoskeleton – 2013).

Podosomes consist of a central core structure primarily composed of F-actin and actin-associated proteins, surrounded by a ring structure of integrins and integrin-associated proteins. Bridging molecules like α-actinin connect the ring and core, while the entire assembly is enveloped by a cloud of mostly monomeric actin molecules (Destaing et al., 2003). Core components of podosomes include F-actin, actin regulators like members of the Wiskott-Aldrich Syndrome protein (WASP) family, the Arp2/3 complex, gelsolin, and cortactin, while the ring structure is associated with adhesion mediators such as paxillin, vinculin, or talin, as well as kinases like PI3K or Pyk2/FAK (Linder and Aepfelbacher, 2003; Buccione et al., 2004).

Integrins anchor podosomes to the extracellular matrix, with β1 integrins predominantly localizing to the core and β2 and β3 integrins to the ring (Linder & Kopp - Journal of Cell Science – 2005).

Recent research has identified an additional cap structure at the top of the podosome core, containing proteins like lymphocyte-specific protein 1 (LSP1), the formin INF2, or α-actinin. This cap likely aids in transitioning the branched actin network of the podosome core to unbranched lateral filaments, influencing actomyosin contractility and mechanosensitivity (Linder and Cervero, 2020; Bhuwania et al., 2012; Cervero et al., 2018) (Linder & Barcelona - European Journal of Cell Biology – 2023).

Furthermore, phosphorylated tyrosine, a characteristic feature of some adhesive structures, was found to be abundant at podosomes, suggesting a regulatory role for cellular tyrosine kinases like Src and Csk (Linder & Kopp - Journal of Cell Science – 2005).

1.4 Phagocytic podosomes

Various research groups have accumulated increasing evidence supporting the presence of F-actin-rich dots exhibiting podosomal characteristics at phagocytic cups. These observations have been made in different cellular models, including primary human macrophages (Labrousse et al., 2011; Ostrowski et al., 2019; Tertrais et al., 2021), murine peritoneal macrophages (Allen and Aderem, 1996), murine bone marrow-derived macrophages (Vorselen et al., 2021), murine bone marrow-derived dendritic cells (Vorselen et al., 2021), the murine macrophage cell line RAW 264.7 (Herron et al., 2022b; Labrousse et al., 2011; Ostrowski et al., 2019; Vorselen et al., 2021), and the human neutrophil cell line HL-60 (Vorselen et al., 2021). These dots have been observed during phagocytosis of various particles, including complement-opsonized zymosan (Allen and Aderem, 1996), latex beads opsonized with complement (Ostrowski et al., 2019) or IgG (Ostrowski et al., 2019; Tertrais et al., 2021), deformable acrylamide beads (Vorselen et al., 2021), as well as in the 2D model of frustrated phagocytosis (Herron et al., 2022b; Labrousse et al., 2011; Ostrowski et al., 2019). It is important to note that individual studies have employed different combinations of phagocytes and ingested particles, thus not all possible combinations have been explored especially that all used models relayed on artificial samples rather than biologically relevant targets. However, a consistent observation is the formation of micron-sized, F-actin-rich dots at the phagocytic cup interface, facilitating close contact between the phagocytic target and the enclosing membrane of the phagocyte. These structures serve as a scaffold for progressive encapsulation and a diffusion barrier for signaling molecules (Linder & Barcelona - European Journal of Cell Biology – 2023).

1.5 Monocytes and macrophages, different phenotypes

Monocytes are a group of cells circulating in the blood, bone marrow, and spleen, and constituting ~10% of the total leukocytes in human beings. Their typical morphological features include an irregular cell shape, oval- or kidney-shaped nucleus, cytoplasmic vesicles, and high cytoplasm-to-nucleus ratio. Monocytes circulate in blood for up to 1–2 days after their maturation and, in case they are not recruited into an infected or malfunctioned tissues, they

would later die and are consequently removed. Monocytes develop in the bone marrow from hematopoietic stem cells (HSCs) and their differentiation involves a series of sequential stages: the common myeloid progenitor (CMP), the granulocyte-macrophage progenitor (GMP), the common macrophage and DC precursor (MDP), and finally the committed monocyte progenitor (cMoP), a recently identified bone marrow precursor that differs from MDP as it lacks CD135 expression. MDP gives rise also to common DC progenitors (CDP), whose differentiation potential is restricted to the DC lineage (Italiani & Boraschi - Frontiers in Immunology – 2014).

Although Monocytes were considered as the systemic reservoir of myeloid precursors for renewal of tissue macrophages and DC, many DC and macrophage subpopulations originate from the MDP independent of monocytes, and in some cases, they can even develop directly from the bone marrow (Italiani & Boraschi - Frontiers in Immunology – 2014).

1.5.1 M1 macrophages

Macrophage polarization occurs through different activation programs by which macrophages carry out their defensive functions. It is known that macrophages can exist in a heal/growth promoting setting where they are designated as M2, which is also the normal "default" program adopted by resident macrophages, or in a setting were they are dedicated to a killing/inhibitory capacity and are designated as M1 macrophages. These two macrophage states are established by modifications in macrophages' metabolic functions, where in M2 macrophages the arginine metabolism is shifted to ornithine and polyamines, which promote cell proliferation, repair, collagen synthesis, fibrosis and other tissue remodeling functions, while in M1 cells it is shifted to NO and citrulline, which are important effector molecules with microbicidal activity and cell proliferation inhibitory capacity. (Italiani & Boraschi - Frontiers in Immunology – 2014) Moreover, M1 and M2 macrophages have distinct features in terms of chemokine production profiles, and iron and glucose metabolism. (Italiani & Boraschi - Frontiers in Immunology – 2014)

1.6 Candida species

Candida spp. are the most common cause of human fungal infections, representing nearly 96% of all opportunistic mycoses. Up to 2% of intensive care unit (ICU) patients suffer from invasive candidiasis, the incidence of which shows an alarming increase during recent years. Overall, *Candida* spp. are the 4th most common cause of hospital acquired bloodstream infections in the United States and 7th in Europe, and approximately 10% of all ICU-acquired bloodstream infections are caused by Candida spp. (Kourkoumpetis et al. - Mycopathologia – 2010).

The genus *Candida* encompasses about 200 species, many of which are harmless commensals or endosymbionts of hosts including humans; however, when mucosal barriers are disrupted or the immune system is compromised they can invade and cause disease, known as an opportunistic infection. Candida is located on most mucosal surfaces and mainly the gastrointestinal tract, along with the skin. (Brandt & Lockhart - Current Fungal Infection Reports – 2012)

1.6.1 *Candida albicans*

Candida albicans is a fungal pathogen that is unique in terms of the diversity of infections it can cause. The main morphotype of C. *albicans* is a yeast shape known as white cells (Pérez et al. - FEMS Yeast Research – 2011). These cells are common in in vitro studies, have a round-to-oval shape, and measure around 5–6 μm (Cottier & Hall - Frontiers in Cellular and Infection Microbiology – 2020). *Candida albicans* is part of the normal resident flora on mucosal surfaces of the gastrointestinal and urogenital tract and is asymptomatic in the majority of humans, however, C. *albicans* has the ability to colonize and invade host tissues in cases of immunodeficiency or disruption of the normal microfloral populations at a given body surface leading in most cases to superficial infections of the mucosal epithelium in gastrointestinal tract, vaginal, or oropharyngeal mucosa. One quite common mucosal infection of C. *albicans* is Recurrent Vulvo Vaginal Candidiasis (RVVC) (Kabir et al. - ISRN Microbiology – 2012). In immunocompromised individuals, infections can progress to a severe systemic invasion, in severely ill patients reaching a mortality rate of about 30% (Kabir et al. - ISRN Microbiology – 2012). In this context, C. *albicans* is the major fungal pathogen in humans (Calderone, 2002),

and recent surveys in the United States have shown that Candida species are the third to fourth most commonly isolated bloodstream pathogen, having surpassed gram-negative rods in frequency as causative agents of septicemia in humans (Pérez et al. - FEMS Yeast Research – 2011).

1.6.2 *Candida auris*

Candida auris was first reported in 2009 and was isolated from the external auditory canal of a Japanese patient as a causative agent of otomycosis (Caliman Sato et al. - GMS German Medical Science – 2023) However, retrospective analysis of preserved strains confirmed that C. *auris* existed in many countries before 2009 and due to challenges associated with its biological identification went eversince unidentified (Wang et al. - Frontiers in Microbiology – 2023).

The environment may be the principal reservoir of C. *auris*, and its morphology of may resemble other, more common, Candida spp.; thus, identification based only on colonies is not possible (Caliman Sato et al. - GMS German Medical Science – 2023)

In their most recent report on antibiotic resistance, the US Centers for Disease Control (CDC) classified C. *auris* as an urgent threat—the highest category. The World Health Organization (WHO) also ranks C. *auris* in the highest prioritization category (Aldejohann et al. - Deutsches Ärzteblatt international – 2023) and this is due to novel characteristics it processes, starting from its high transmissibility via direct and indirect contact (hands, medical devices, near-patient environment including walls and floor contact) that cause nosocomial outbreaks that are difficult to control, in addition to its high tenacity lasting for 4–14 days, as well as its resistance to several antifungal drugs, where more than 80% of all isolates are resistant to fluconazole, and are less susceptible to other azoles and 10% to 30% of all isolates have reduced susceptibility to amphotericin B as well as echinocandin (Aldejohann et al. - Deutsches Ärzteblatt international – 2023) additionally, *Candida auris* poses a high risk of causing bloodstream and other disseminated infections as well as propensity to cause outbreaks due to its difficult identification and its transmission that occurs through contaminated surfaces and equipment, such as patient-care equipment (stethoscopes, thermometers, etc.) which in its turn leads to the endangerment of patients with immunosuppression or immunodeficiency, as

in the case of Covid-19, HIV or after transplantation (Caliman Sato et al. - GMS German Medical Science – 2023)

1.7 Working hypothesis/ research question

Previous research in the field of phagocytosis, actin cytoskeletal rearrangements in M1 macrophages suggests cytoskeletal modifications that occur during uptake of foreign particles in a process that starts with actin filaments organizing as a dense meshwork underlying the plasma membrane in a structure called the phagocytic cup after which, actin re-organizes progressively all around the particle until closure of the phagosome membrane (Krendel & Gauthier - Current Opinion in Cell Biology – 2022). The phagosome then undergoes a maturation process, where it progressively loses its F-actin coat for the abundance of actin around the phagosome determines its capacity to fuse with lysosomes (Nguyen & Yates - Frontiers in Immunology – 2021).

In experiments condcuted with Zymosan and opsonized latex beads, podosome-like structures have also been observed at these phagocytic cups. In contrast to what was previously noted where the F-actin distribution within a phagocytic cup is uniform and continuous, it appears that the phagocytic actin structure rather comprises discreet podosome-like dots that wrap around the injested particle. These podosome-Like structures were then further investigated with the help of an artificial model as latex beads, for their exact localization, their correlation with matrix-associated podosomes, the formation of phagolysosomes, and their dependence on the characteristics of the ingested particle. (Tertrais et al. - European Journal of Cell Biology – 2021).

Research findings suggest that these podosome like structures identified at phagosomes are phagocytic podosomes that share many of matrix associated podosomes' characteristics in terms of composition and structure, additionally, it was suspected that these structures may carry a function that corrolates with phagolysosome fusion (Tertrais et al. - European Journal of Cell Biology - 2021).

Despite the identification of these podosome-like structures and their initial investigation, it remains unknown whether the previously carried, artificial model phagocytosis experiments hold firm with actual biological samples and occur in living organisms, moreover little is known about the characteristics of these structures and the discrepancies that differentiate them from matrix associated podosomes. In addition to that, their exact role within the phagocytic process, and their role in phagolysosome maturation remains not thoroughly investigated.

In this project I aim to answer the following questions:

1- Do phagocytic podosomes occur on phagosomes formed around living biological samples?
2- What are the major characteristics of these structures in terms of composition, structure, function, lifespan, and chemical inhibition susceptibility/resistance?

2. MATERIALS AND METHODS

2.1. Materials

2.1.1. Devices

Table 2 Devices

Devices Type	manufacturer
Autoclave Bioclave,	Bioclav, Schütt Labortechnik GmbH, Göttingen Varioklav MediTech, Norderstedt
Ice machine	Flake ice maker AF-10, Scotsman, Vernon Hills, Illinois, United States of America, Hoshizaki Ice Maker, Hoshizaki Electric Co., Ltd., Japan
Precision scale	Sartorius AG, Göttingen
Incubator for cell cultures	CO2 incubator MCO-20AIC, 215 liters, Ewald Innovations Technik GmbH, Bad Nenndorf
Magnetic stirrer	RH Basic 2, IKA®-Werke GmbH & Co. KG, Staufen
Electroporation system for eukaryotic cell	NEON® Transfection System, Life Technologies, Carlsbad, California, United States of America
pipettes	2, 10, 20, 100, 200, 1000 µl, and Multipipette by Eppendorf Vertrieb Deutschland GmbH, Cologne/Wesseling; Accu-jet pro, Brand, Wertheim
Tweezers	neoLab Migge Laborbedarf-Vertriebs-GmbH, Heidelberg
Shaker	KL2, Edmund Bühler, Tübingen

Magnetic separation columns	µMACS TM Separator Miltenyi Biotech, Bergisch Gladbach
magnetic stirrer	MR 3001, Heidolph, Schwabach
shaker	Vortex REAX top, Heidolph, Schwabach
balance	440-47N, Kern, Balingen-Frommern
cell counter	Neubauer Chamber, Hartenstein, Würzburg
Centrifuge	5417R and 5810R, Eppendorf Vertrieb Deutschland GmbH, Cologne/Wesseling; Benchtop centrifuge, neoLab, Heidelberg
Cell culture dishes	150x20 mm, Sarstedt, Nümbrecht

2.1.2 Microscopes

Table 3 Microscopes

Light microscope	
Provider	Nikon, Tokio, Japan
Model	Eclipse TS100
Objective	Plan Fluor 4x / 0.13 PhL LWD 10x / 0.25 Ph1 LWD 20x / 0.4 Ph1 LWD 40x / 0.55 Ph1

Camera	Nikon D5000 Digitalkamera
Emission filter	Filter set HQ EGFP (green) / HQ Calcium Crimson, Chroma Technology, Rockingham, North Carolina, USA
UV lamp	Nikon Intensilight 130 W mit Halogenlampe
Halogen lamp	Standard housing with 30 W

Olympus FV3000

Microscope	**Olympus IX83**
Objectives	2x PlanApo N NA: 0.08 WD (=working distance; mm): 6.2
	4x UPlanXApo (optionally available) NA: 0.16 WD (mm): 13
	10x UPlanXApo NA: 0.40 WD (mm): 3.1
	20x UPlanXApo NA: 0.8 WD (mm): 0.6
	30x UPlanSApo Sil Coverglass (mm): 0.13-0.19 NA: 1.05 WD (mm): 0.8
	40x UPlanXApo (optionally available) Coverglass (mm): 0.11-0.23 NA: 0.95 WD (mm): 0.18
	60x UPlanSApo Sil (optionally available) Coverglass (mm): 0.15-0.19 NA: 1.3 WD (mm): 0.3

	60x PlanApo N SC Oil Coverglass (mm): 0.13-0.19 NA: 1.50 WD (mm): 0.11
Detectors	High Sensitivity Spectral Detector with 4x GaAsP PMT, 1x Trans PMT
Laser lines (nm)	Solid state: 405 / 445 / 488 / 514 / 561 / 594 / 640
Pinhole size	variable
Spectral separation	Motorized Volume Phase Holographic (VPH) transmission diffraction grating
Hybrid-Scanner	Galvo: 512x512 @ 1 fps (16 fps interlaced mode); Tornado scanning for fast ROI scanning
	Resonant: 512x512 @ 30 fps; max. speed: 512x32 @ 438 fps
Software	Olympus FV-3000
Filters for fluorescence	Filtersystem (em.-color, dye): excitation | emission
	Triple filter cube DAPI/FITC/TRITC (Chroma 69000):
	DAPI: 392 - 416 nm | 440 - 462 nm FITC: 473 - 495 nm | 543 - 561 nm TRITC: 507 - 533 nm | 574 - 618 nm
UV-VIS illumination	CoolLED pE-300white
Transmitted light	LED (IX3-LHLEDC)
Contrast enhancement	Differentiel interference contrast (DIC)
CO2 controller	Cell vivo CB1G
Temperature controller	Cell vivo CBT with Pecon heating unit 2000

Large incubation chamber	Cell vivo/Pecon
Mini-incubation chamber for PiezoZ	Cell vivo/Pecon
Actively damped optical table	Newport Vision IsoStation

Visitron SD-TIRF

Microscope	**Nikon Eclipse TiE**
Objectives	10x CFI Plan Fluor DL Phase NA: 0.30 WD (mm): 15.2 Pixel size in image (µm): 1.100
	20x CFI Plan Fluor DLL Phase NA: 0.51 WD (mm): 2.1 Pixel size in image (µm): 0.550
	40x Plan Fluor Phase NA: 0.75 WD (mm): 0.66 Pixel size in image (µm): 0.275
	40x CFI Plan Fluor Oil NA: 1.30 WD (mm): 0.2 Pixel size in image (µm): 0.275
	60x Apo TIRF (corr.) Oil NA: 1.49 WD (mm): 0.13 (CS: 0.10-0.22 @ 23 or 37 °C) Pixel size in image (µm): SpinningDisk: 0.183; SORA disk: 0.065
	100x CFI Plan Apo Lambda

	NA: 1.45 WD (mm): 0.13 Pixel size in image (µm): spinningDisk: 0.110; SORA disk: 0.039
Cameras	2x Photometrics Prime 95B (back-illuminated sCMOS, 11µm pixel-size, 1200x1200 pixels)
Laser lines (nm)	Solid-state: 405 / 445 / 488 / 515 / 561 / 640
Spinning Disk unit	Yokogawa CSU W-1 SoRa in dual-camera configuration 1) Confocal disk (50µm pinholes) 2) SoRa disk for super-resolution
Emission filters spinning disk (for laser-related fluorescence)	Camera 1: DAPI, 460/50 CFP, 470/24 GFP, 525/50
	Camera 2: YFP, 535/30 mCherry, 609/54 CY5, 700/75
Dichroic in spinning disk unit	561LP 514LP
Fluorescence filters in microscope stand	Filtersystem (em.-color, dye): excitation | beamsplitter | emission DAPI (blue; DAPI): BP 325-375 | DM 400 | BP 435-485 GFP (green; AF488, GFP): BP 450-490 | DM 495 | BP 500-550 TxRed (red; AF568, mCherry): BP 540-580 | DM 585 | BP 593-668

Dichroic mirrors in microscope stand for TIRF and FRAP	TIRF-FRAP1: 405/488/561/640 rpc BS (Chroma; 2mm) TIRF-FRAP2: 442/514 rpc BS (Chroma; 2mm
UV-VIS illumination	SOLA-SM Light Engines, white light LED, 380-680nm
Transmitted light lamp	precisExcite, High-Power 525nm LED
Software	VisiView v4
Incubation unit	okolab bold line
FRAP-TIRF unit	Roper iLAS2 for FRAP&TIRF with all laser lines
Piezo focus drive	Ludl NanoPrecision PiezoZ, 350µm travel range
Motorized XY stage	Ludl BioPrecision3 LM
Auto-focus	Nikon PerfectFocus system
Actively damped optical table	Newport

2.1.3. Software

Table 4 Software

Software	Provider
Excel Software	Microsoft, Redmond, Washington, USA
GraphPad Prism 5	GraphPad Software, Inc, La Jolla, Californien, USA
ImageJ	Bethesda, Maryland, USA

2.1.4 Consumables

2.1.4.1 Antibodies

2.1.4.1.1 Primary antibodies

Table 5 Primary antibodies

Antigen	Donor species	Polyclonal/monoclonal	producer
Arp2	mouse	IgG1	Abcam-ab49674
Cortactin	mouse	polyclonal	BD-610035
Vinculin	mouse	polyclonal	Sigma
LSP1	mouse	IgG1	BD Transduction 610734
Gelsolin	mouse	IgG1	Transduction Lab. Cat. No G37820
PY99	mouse	Polyclonal	Santa Cruz
Myosin 9	rabbit	polyclonal	Santa Cruz
MT1MMP	mouse	monoclonal	Invitrogen
Myosin 1F(B-5)	mouse	monoclonal	Santa Cruz sc-376534
Talin 2	mouse	IgG2a	Sue Monkley
ß1-Integrin	mouse	IgG	Santa Cruz Biotechnology sc-73610
STIM1	rabbit	IgG	Cell Signaling #5668
Tks5	rabbit	polyclonal	Ronald P Leon, Portland MABT336

DNAseX	mouse	IgG1	Abnova H0001774-M02
α-actinin	mouse	IgG	Santa Cruz Biotechnology sc-17829
Cortactin Alexa 555, clone4F11	mouse	IgG1	Upstate Cat.16-229 1:100

2.1.4.1.2 Secondary antibodies

Table 6 Secondary antibodies

Antigen	Donor species	Species against	Polyclonal/Monoclonal	Producer
Donkey Anti-Mouse Alexa 405	donkey	mouse	IgG H&L	abcam ab175658
goat anti-mouse Alexa 488	goat	mouse	IgG (H+L)	Invitrogen (A11001)
donkey anti-mouse Alexa 568	donkey	mouse	IgG (H+L)	R&D (NL007)
donkey anti mouse	donkey	mouse	IgG(H+L)	abcam ab175658
donkey anti-rabbit Alexa 568	donkey	rabbit	IgG (H+L)	molecular probesA10042

donkey anti-rabbit Alexa 647	donkey	rabbit	IgG (H+L)	molecular probes A31573
goat-anti rabbit Alexa488	goat	rabbit	IgG(H+L)	Jackson 111-545-003
Donkey Anti-Rabbit (Alexa Fluor 405)	donkey	rabbit	IgG H&L	abcam ab175651

2.1.4.2 Chemicals and consumables

Table 7 Chemicals and consumables

Consumable	**Type, producer**
PP2	Millipore- 529576-1MG
DMSO	Finzymes- F-515

Kits, enzymes, agents	**producer**
Transfection system	Neon®Transfection System, Invitrogen/Life Technologies, Carlsbad, California, USA
Macrophage detachment medium	Accutase TM Enzyme Cell Detachement Medium,eBioscience, Inc., San Diego, California, USA
Triton™ X-100	Sigma-Aldrich Chemie GmbH, Steinheim
Mowiol® 4-88	Sigma-Aldrich Chemie GmbH, Steinheim
Formaldyhyde	VWR Chemicals

Cell culture media	**provider**
RPMI	GIBCO® RPMI, Thermo Scientific, Rockford, Illinois, USA
Monomedium	Universitätsklinikum Eppendorf, Hamburg
Lymphocyte Separations Medium (LSM)	PAA laboratories, Somerset, England

Additives/ antibiotics	**provider**
Streptomycin/ penicillin	Sigma-Aldrich Chemie GmbH, Steinheim
Bovine serum albumin (BSA)	Sigma-Aldrich Chemie GmbH, Steinheim
Human serum	Universitätsklinikum Eppendorf, Hamburg

Additives/ buffers	**Composition**
DPBS (1x)	GIBCO® Dulbecco's Phosphate Buffered Saline, Thermo Scientific, Rockford, Illinois, USA.
PBS (10x)	KCl Na2HPO4 KH2PO4 ddH2O pH 7.7
Monocyte buffer	PBS EDTA human Serum albumin) pH 7,4 1x 5 mM 0,5 %

2.1.4.3 Plasmids

Table 8 Plasmids

Vector	Plasmid Type
MT1-MMP mCherry E.coli DH5α HindIII/XbaI Amp	PCDNA3.1
LifeAct GFP E.coli DH5α Kan	pEGFP-N1

2.1.4.5 Cells

Table 11 cells

Cells	Characteristics
Macrophages	Human origin, from donor blood
Candida auris	From Universitätsklinikum Eppendorf, Hamburg
Candida albicans	From Universitätsklinikum Eppendorf, Hamburg

2.2 Methods

2.2.1 General methods

All cell culture work was performed under sterile conditions in a sterile cabinet (safety cabinet, Hera Safe, Thermo Scientific, Rockford, Illinois, United States of America) and cells were cultured in an incubator (CO2 incubator MCO-20AIC, 215 liters, Ewald Innovations Technik GmbH, Bad Nenndorf, Germany) at 4 % CO2 concentration, 90 % humidity and 37°C.

All media and solutions that were not already purchased sterile were sterilized for cell culture with a 0.2 µm filter membrane filtration system (Stericup, Millipore, Bedford, United States of America) connected to a vacuum pump or with a 0.2 µm syringe filter (SFCA 0.2 µm, Thermo Scientific, Rockford, Illinois, United States of America).

2.2.2 Monocytes/macrophages

Primary human monocytes/macrophages were isolated weekly from fresh blood. The cell culture medium used was RPMI (Thermo Scientific, Rockford, Illinois, United States of America) with 20% human serum and 1% penicillin/streptomycin (Sigma-Aldrich Chemie GmbH, Steinheim, Germany). The duration of differentiation of monocytes to macrophages by factors in human serum is approximately 7 days.

2.2.2.1 Preparation of monocytes

The monocytes were prepared from the buffy coats. For this purpose, 20 ml of blood was carefully layered onto 15 ml of cold lymphocyte separation medium (PAA laboratories, Somerset, England) and then centrifuged for 30 min at 1500 rpm and 4°Celsius without a brake (5810R, Eppendorf Vertrieb Deutschland GmbH, Cologne/Wesseling). The lymphocyte layer was then collected in 10 ml of cold RPMI medium and a new centrifugation step followed, for two times 10 min each at 1500 rpm and 4°Celsius with brake. The supernatant was discarded and the pellet was taken up in approx. 10 ml of cold RPMI. Subsequently, centrifugation was repeated for 10 min at the same parameters and the cell pellet was collected in 1.5 ml of cold monocyte buffer stored on ice with the addition of 250 µl CD14 antibody-coupled magnetic beads for cell separation (CD14 MicroBeads MACS, Milteny Biotec GmbH, Bergisch Gladbach), and incubation on ice for 15 minutes. By applying the solution to magnetic separation columns (µMACS TM Separator Miltenyi Biotech, Bergisch Gladbach), the cells bound to the magnetic beads were separated from the remaining cells. These were taken up at a cell concentration of

$1.5x10^6$ cells/ml in RPMI medium and 1 ml per well was added to a 6-well plate (Sarstedt, Nümbrecht), which was then incubated for 4 hours in an incubator. After adhesion of the cells, the medium was removed and replaced with cell culture medium (RPMI with 20 % autologous serum, 1 % penicillin/streptomycin). The macrophages were used at the earliest after differentiation of the monocytes into macrophages after approximately 7 days.

The macrophages were assessed objectively before use and only those with a uniform shape were selected. Care was taken to ensure that predominantly round-shaped phenotypes dominated the culture.

2.2.2.2 Cell culture monocytes/macrophages

The monocytes/macrophages were cultivated at a cell concentration of $1.5x10^6$ cells with 1.5 ml cell culture medium per well of a cell culture plate with a growth area of 8.87 cm^2.

2.2.2.3 Detachment of the macrophages

After aspiration of the culture medium, the cells were washed once with 1x DPBS (Dulbecco's Phosphate Buffered Saline, Thermo Scientific, Rockford, Illinois, United States of America) and then incubated with 500 µl detachment medium for macrophages (Accutase TM Enzyme Cell Detachment Medium, eBioscience, Inc., San Diego, California, United States of America) per well of a 6-well plate with approximately 400,000 detached cells for 15 min in the incubator. The Accutase and DPBS were heated to 37°C. After detachment, the cells were centrifuged for 5 min at 1500 rpm (5810R, Eppendorf Vertrieb Deutschland GmbH, Cologne/Wesseling), the cell pellet was collected in DPBS and the cell count was determined using a Neubauer chamber (Hartenstein, Würzburg). After a further centrifugation, the pellet was taken up at the desired cell concentration in 37°C warm culture medium.

2.2.2.4 Transfection of macrophages

Transfection of macrophages with DNA-constructs for target proteins was performed on 10^5 cells per well in an electroporation system for eukaryotic cells (NEON® Transfection System, Life

Technologies, Carlsbad, California, United States of America), according to the manufacturer's instructions and the electroporation parameters in Table 12. Stuffed pipette tips (Sarstedt, Nümbrecht, Germany) were used.

	Voltage (V)	Pulse duration (ms)	Number of pulses	Cell density	Tip (ul)
Macrophages	1000	40	2	10~6	100

2.2.3 Candida preparation

Candida species were cultivated on agar plates and stored in the fridge at 4°C . Using an inoculation loop and in close proximity with a Bunsen burner a few colonies of candida were removed and immersed in a 1ml vile containing PBS. The solution was then centrifuged for 8 min at 14000 rotations and temperature 30°C. The supernatant was discarded and the pellet was dissolved in RPMI.

To determine the concentration of Candida/RPMI medium, 4 dilutions of the Candida-RPMI solution ranging from 1:10 to 1:10000 respectively were performed. On C-chips, 10µl from every diluted vile are added and the number of Candida seen under the light microscope in designated area of the chips was counted.

The Concentration of initial Candida-RPMI solution is then estimated according to the following formula: number of candida seen on C-chip x 10^4x dilution concentration in diluted vile = concentration of Candida in initial solution

The infection of macrophages was done according to an MOI of 20 Candida per macrophage and the Candida infection solution is prepared according to the following formula.

Nb of cells (macrophages) x MOI = Nb of Candida needed

Volume of Candida needed = Nb of Candida needed\concentration of Candida solution (determined from the counting)

The volume of Candida solution is then pipetted into a vile that is then filled up with RPMI to reach the needed volume per number of coverslips (300µl per coverslip).

2.2.4 Infection of Macrophages with Candida species

Macrophages were grown in 12 well plates on 8mm coverslips and left in the incubator in 100µl monomedium under 5%CO2 and at a temperature of 37°C.

The monomedium was then discarded away from the coverslips with the help of a bench suction tube and 300µl of the prepared Candida solution is added to each coverslip in a well.

The 12 well plates were then centrifuged for 3min at 1000 rotations at 30°C

The plates were put back into the incubator and left there for a time interval depending on time post infection needed (5-10-20-40-60 minutes)

When the target time post infection is reached, the RPMI-Candida solution was discarded using a bench suction tube from the coverslips in the wells and formaldehyde was added to fix the cells.

The coverslips were then left in formaldehyde for 10-20min

Formaldehyde was later removed and replaced 0.5ml PBS in each well before the plates were stored in the fridge at (4°C) untill the time of staining.

2.2.5. Fluorescent staining

Samples were incubated for 10 min with PBS containing either 0.1–0.25% Triton X-100 (or 100 µM digitonin or 0.5% saponin). Cells were then washed in PBS three times for 5 min. Cells were then incubated with 1% BSA or 10% serum from the species the secondary antibody was raised in (typically goat serum, or donkey serum), for 30 min in a humidified chamber at room temperature or overnight at 4°C.

The solution was then decanted and the cells were washed three times in PBS, with 5 min for each wash.

Cells were later Incubated cells with Phalloidin (for F-actin staining) and DAPI (for DNA staining) in 1% BSA or other specific serum solution for 1 h at room temperature in a dark humidified chamber.

The coverslips were then washed three times with PBS for 5 min each.

Coverslips were then mounted on microscopy slides with a drop of mounting medium (Moviol).

Coverslips were sealed with nail polish to prevent drying and movement under microscope.

Coverslips were finally stored in the dark at +4°C.

2.2.6 Immune-fluorescent staining

Samples were incubated for 10 min with PBS containing either 0.1–0.25% Triton X-100 (or 100 µM digitonin or 0.5% saponin). Cells were then washed in PBS three times for 5 min. Cells were then incubated with 1% BSA or 10% serum from the species the secondary antibody was raised in (typically goat serum, or donkey serum), for 30 min in a humidified chamber at room temperature or overnight at 4°C.

The solution was then decanted and the cells were washed three times in PBS, with 5 min for each wash.

Cells were later Incubated with the primary antibody in 1% BSA or other specific serum solution for 1 h at room temperature in a dark humidified chamber.

The primary antibody solution was then decanted and washed three times with PBS for 5 min each.

Cells were later Incubated with the secondary antibody in 1% BSA or other specific serum solution for 1 h at room temperature in a dark humidified chamber.

The secondary antibody solution was then decanted and washed three times with PBS for 5 min each.

Coverslips were then mounted on microscopy slides with a drop of mounting medium (mowiol).

Coverslips were sealed with nail polish to prevent drying and movement under microscope.

Coverslips were finally stored in the dark at +4°C.

2.2.7 live cell imaging

Infections of macrophages with candida species were performed in incubation chamber at 37°C and 5%CO2 using Visitron SD-TIRF microscope and the infection media were recorded at different channels (green, Red, Cyan and bright field) with full cell stacks taken within a time interval t=30sec per stack over an interval of 30min. Collected data about phagocytic podosomal lifetime were then analyzed using descriptive statistical methods.

2.2.8 Chemical inhibition of cellular proteins

Macrophages were prepared on coverslips with 10^5cells/coverslip in 12 well plates and left to starve for 2hrs in RPMI. DMSO (25 µM)-RPMI and PP2(25 µM)-RPMI solutions were added to 2 separate groups of cells in 2 different 12 well plates and cells were left in this incubation medium for 10min before starting the candida infection. Coverslips in both mediums were retrieved at 5, 10, 20,40, 60 min after infection respectively and fixed in formaldehyde. The collected data from matrix podosome and phagocytic podosome quantification in both cell media were then analyzed using multiple unpaired t-tests with P-values <0.05 considered of statistical significance.

.

3-RESULTS

3.1 Actin Foci on Candida Phagosome

Macrophages were infected with *Candida albicans* and *Candida auris* cells, respectively, according to the mentioned protocols, followed by fluorescent staining for F-actin using Phalloidin 488 for the investigation of actin rearrangements during phagocytosis , both at phagosomes and at the ventral surface of macrophages that contains matrix-associated podosomes. Fluorescent and bright field microscopy using SORA-Visitron (Super Resolution via Optical Re-assignment) revealed micron-sized F-actin foci localized around candida phagosomes that are presented in Figure 1A.

A 3D representation of these F-actin foci around a *Candida auris* phagosome with matrix associated podosomes in the background is represented in Figure 1B.

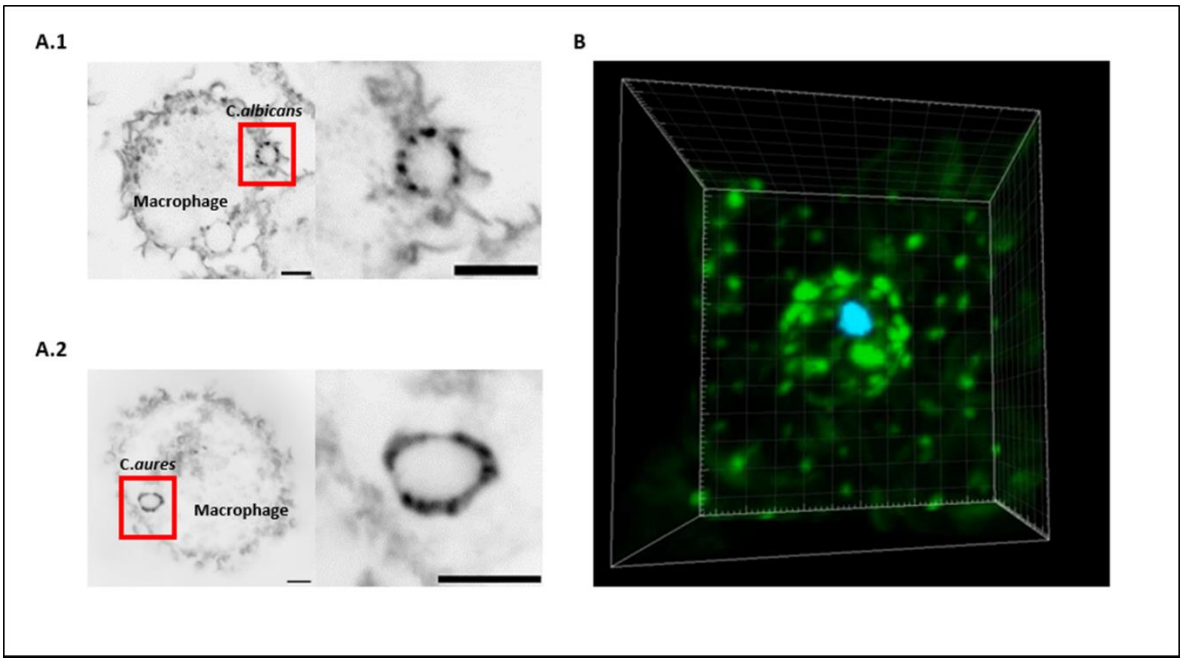

Figure 1: Microscopic images of phagocytosis of *Candida species*. A.1-Phagocytosis of *Candida albicans* by a primary macrophage stained using phalloidin 488 (green) depicting the actin foci around the Candida phagosome, with a zoom-in view of areas indicated by red boxes. A.2-Phagocytosis of *Candida auris* by a primary Macrophage stained using phalloidin 488 (green) with actin foci around Candida phagosome with a zoom-in view. B-a 3D view of a *Candida auris* phagosome in a Primary macrophage with F-actin foci shown in green (phalloidin 488 staining for F-actin) and Candida nucleus shown in Cyan (DAPI 405) with matrix associated podosomes appearing in the background towards the ventral surface of the cell.

3.2 Identification of main Protein composition of Podosome-Like Structures

In order to investigate the structural similarity between Actin foci present on Candida phagosomes' surface and matrix associated podosomes that are constitutively expressed on ventral surface of macrophages, immunofluorescence staining of several target proteins was performed. These proteins are known to form the core, ring and cap structures of matrix podosomes. In these experiments, macrophages were fixed 20min post infection with Candida whereby Candida phagosomes are best enclosed within the cell and clearly demarcated.

Immunofluorescence staining targeted specific proteins that belong to the core structure of matrix podosomes such as F-actin, cortactin, gelsolin, and Arp2 in addition to others that were found to be inherent to the ring structure such as vinculin as well as cap proteins such as LSP1 and a-actinin. The results of these stainings in relation to F-actin foci along with their intensity curves are represented in figure 2.

Signals from matrix associated podosomes' core proteins such as Cortactin, Gelsolin and Arp2 appeared to overlap with F-actin signals with intensity curves showing simultaneous peaks at these actin foci, additionally signals from PY99 (phosphorylated tyrosine) that is usually associated with high tyrosine kinase activity that is described to occur at matrix associated podosomes were also overlapping with signals of F-actin at the distinguished actin foci with intensity curves showing simultaneous peaks of both signals at these areas.

Signals from LSP1 and and α-actinin, which are described to be proteins of matrix associated podosomes' cap structure also showed and overlapping pattern with F-actin signals at the identified F-actin foci with intensity curves showing simultaneous overlapping peaks.

Signals from Vinculin and Myosin9 that are known to be part of the surrounding ring matrix associated podosomal structure showed a mutually exclusive signal pattern with F-actin signals at actin foci, and were rather distributed around these foci. Additionally, intensity curves of these protein signals and F-actin showed an F-actin peak accompanied by a Vinculin/Myosin9 trough that is directly surrounded by Vinculin/Myosin9 peaks.

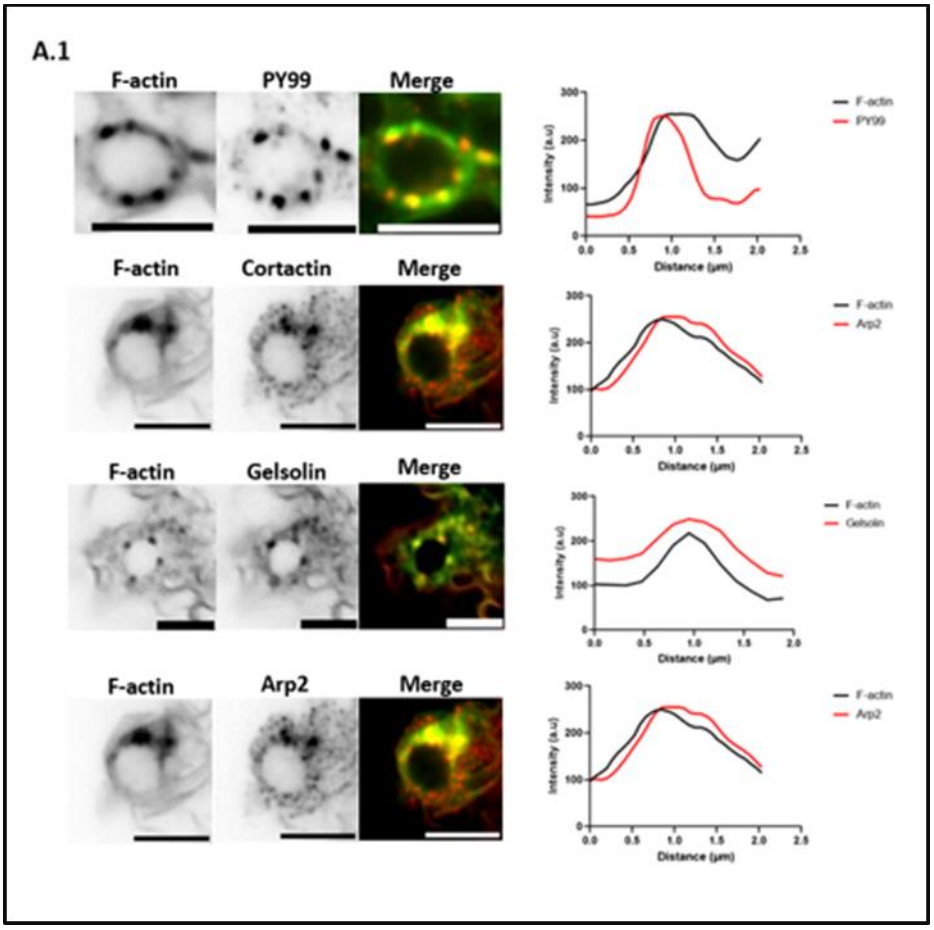
A.1
F-actin
PY99
Merge
F-actin
Cortactin
Merge
F-actin
Gelsolin
Merge
F-actin
Arp2
Merge
Intensity (a.u)
Distance (µm)
F-actin
PY99
Arp2
Gelsolin

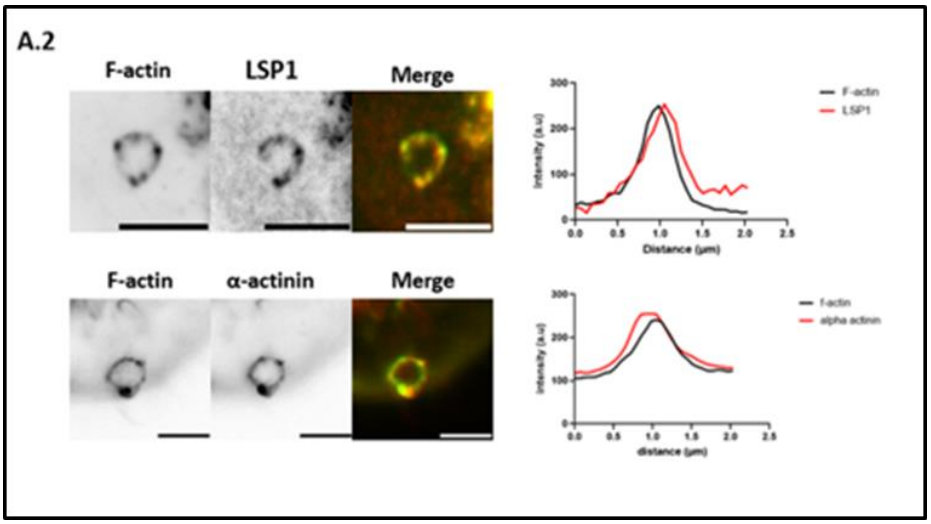
A.2
F-actin
LSP1
Merge
F-actin
α-actinin
Merge
Intensity (a.u)
Distance (µm)
distance (µm)
F-actin
LSP1
alpha actinin

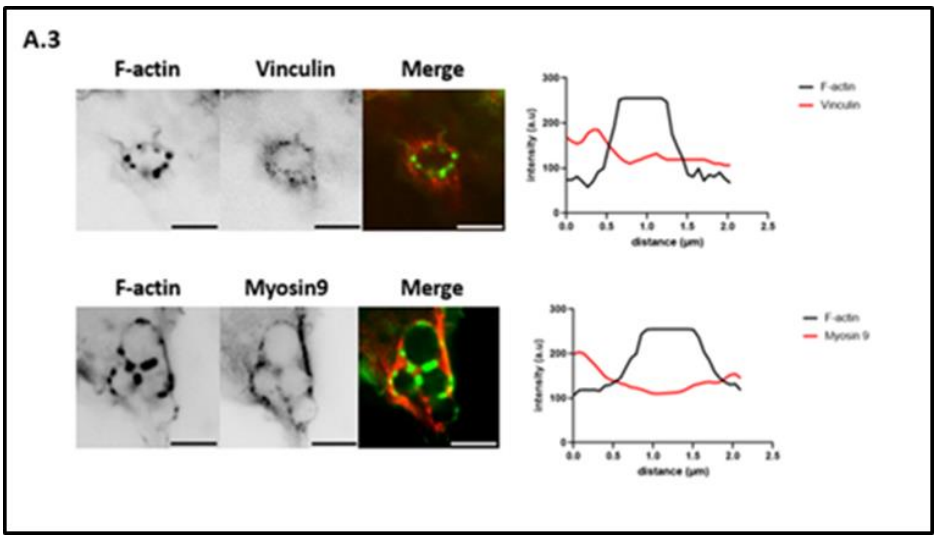

Figure 2: immunostaining of core, ring, and cap proteins of matrix podosomes at Candida phagosomes. A.1-Candida phagosomes stained with phalloidin 488 (green) for F-actin along with immune-staining with secondary alexa fluor 566 (red) staining of the matrix podosome core-associated proteins cortactin, gelsolin, Arp2 and the phosphorylated aminonacid phosphotyrosine PY99 respectively, with merged channels showing their localization with respect to F-actin with colocalisations appearing in yellow as well as their corresponding signal intensity curves. A.2- Candida phagosomes stained with phalloidin 488 (green) for F-actin along with immune-staining with secondary Alexa fluor 566 (red) staining of the matrix podosome cap-associated proteins LSP1, α-actinin respectively, with merged channels showing their localization with respect to F-actin with colocalisations appearing in yellow as well as their corresponding signal intensity curves. A.3-Candida phagosomes stained with phalloidin 488 (green) for F-actin along with immune-staining with secondary alexa fluor 566 (red) staining of the matrix podosome ring-associated proteins vinculin, and myosin9 respectively, with merged channels showing their localization with respect to F-actin with colocalisations appearing in yellow as well as their corresponding signal intensity curves.

3.3 Tracking Podosome-like structures on Candida Phagosome

In order to investigate the characteristics of these F-Actin foci occurring on candida phagosomes, an experiment was conducted in which Candida phagosomes were tracked throughout a time interval in which these actin foci are identified at their first appearance and tracked up to the time of their disappearance with the help of live cell imaging. This tracking procedure is illustrated in figure 3.

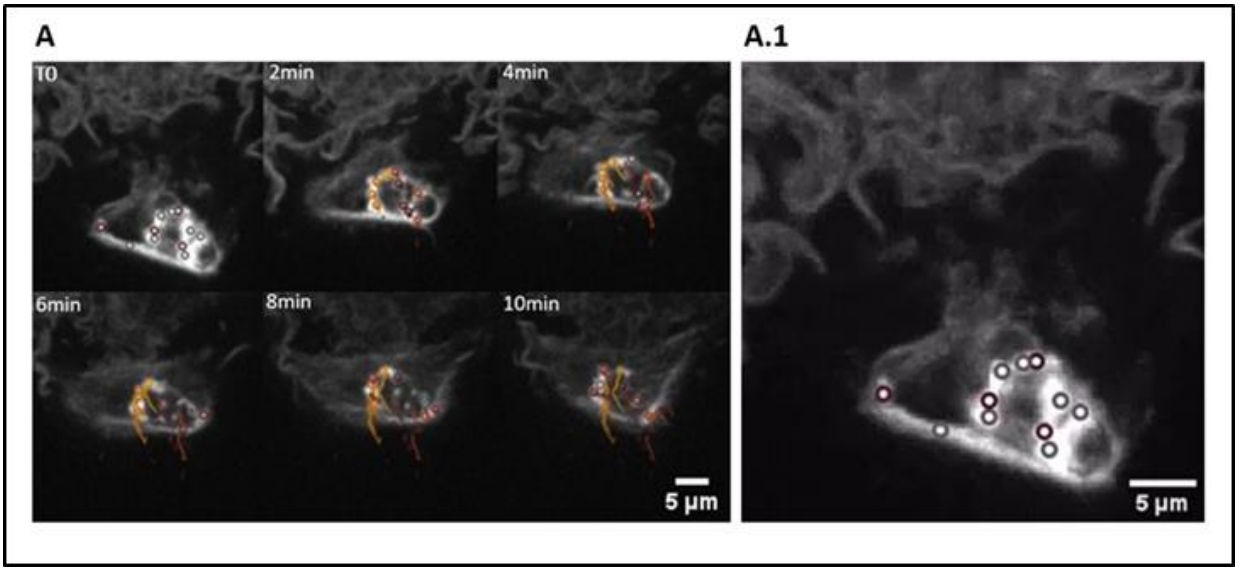

Figure 3: Tracking of phagosome-associated F-actin foci over time. 3.A-Microscopic images using live-cell imaging of macrophages expressing lifeact-GFP (green) visualizing F-actin foci around a Candida phagosome and displaying the trajectory of these foci over a time interval of 10min with still images from times 0,2,4,6,8, and 10min of infection respectively. 3.A.1- a zoom-in view of Candida phagosomes at time 0 showing F-actin foci to be tracked.

Results regarding the lifespan distribution of these F-actin foci and their frequency distribution as a function of lifespan are represented in figure 4 whereby the average lifespan of phagosome associated F-actin foci was 1.65min with a SD of 2.06 min and a distribution ranging between 0 and 18min lifespan of different F-actin foci. Additionally, the frequency distribution on the right shows that up to 60% of phagosome associated F-actin foci had a lifetime of 1 min with this percentage decreasing as lifetime of foci increased where less than 1 % of foci had a lifetime of more than 5min.

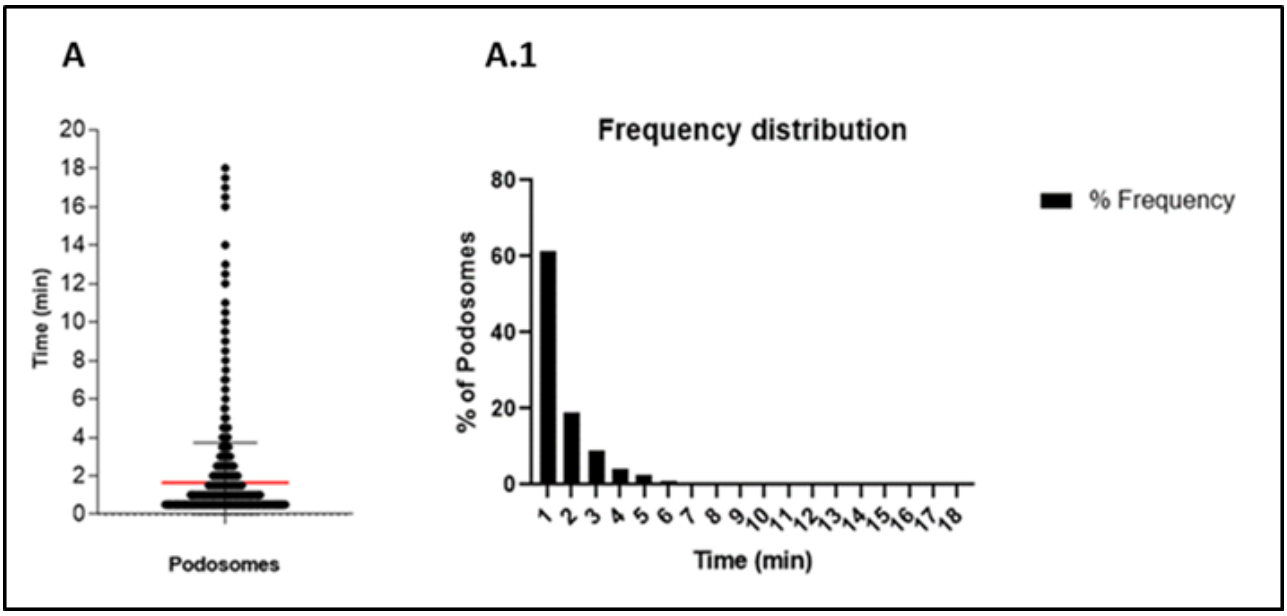

Figure 4: Lifespan distribution of phagosome associated F-actin foci. A.1-Frequency distribution (%) of phagosome associated F-actin foci according to their respective lifespan. These results were obtained by descriptive statistical methods analysing 916 phagocytic podosomes identified in *Candida auris* - infected macrophages from 3 different donors over a time interval of 30min post infection. Median=1min, Mean=1.65min, Std. deviation=2.06min.

In another experiment, and to investigate further characteristics pertaining to the time of appearance of these F-actin foci on phagosomes during the process of phagocytosis and their respective abundance on phagosomes at several time points during this process, an experiment was designed in which phagosome associated F-actin foci were quantified at different times of infection (5-10-20-40-60)min respectively in macrophages from 3 different donors. The results presented in figure 5 showed that 60% of phagosomes acquired at least 1 F-actin focus after 5 min of infection, the level of phagosomes with podosomes increased to reach a peak of 80% at 10min after infection and decreased to 60% at 20min and 30% at 40min after infection and F-actin foci were almost completely disappeared after 60 min of infection. In another quantification , the average number of F-actin foci per phagosome was around 3.6 foci/phagosome at 5, 10, and 20 min respectively and fell to zero at 40 and 60 min of infection as shown in figure 5A.1.

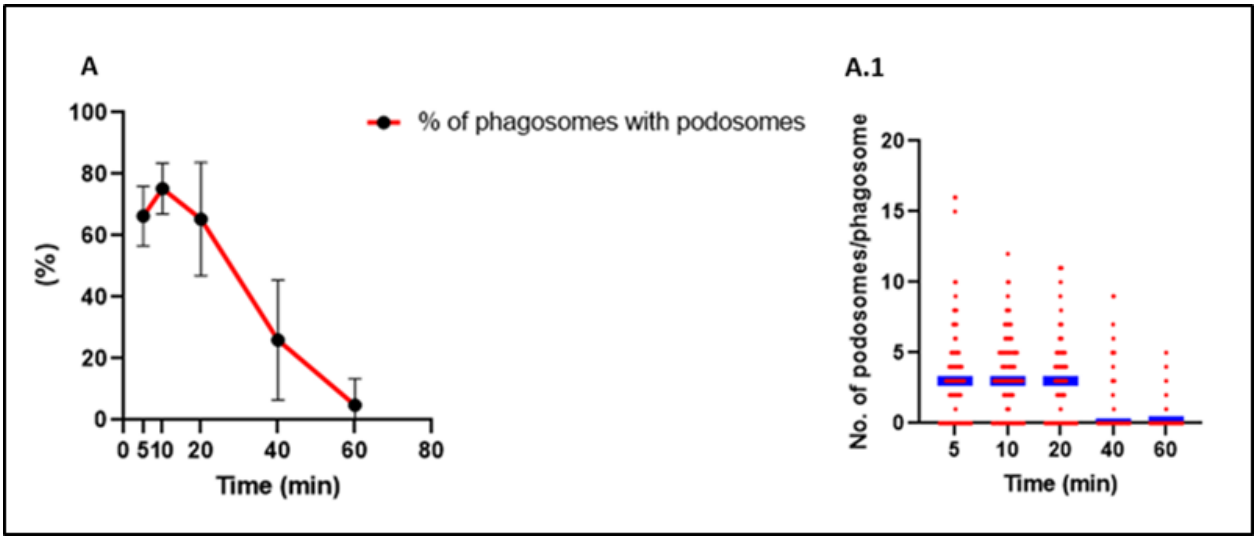

Figure 5: Graphic representation of the variation of percentage of phagosomes with F-actin foci as function of time post infection. A.1-the variation in the number of F-actin foci per phagosome as a function of time after infection. These results were obtained by descriptive statistical methods analysing phagocytic podosomes identified in *Candida auris* - infected macrophages from 3 different donors over a time interval of 60min post infection.

3.4 Association of phagosome associated F-actin foci with degradative enzymes.

In order to investigate the possible association of these phagosome specific F-actin foci with degradative enzymes, a fluorescently labelled construct of MT1-MMP (MT1-MMP-mCherry) was overexpressed in primary macrophages along with lifeact for visualization of F-actin. The infection with *Candida auris* was then closely monitored using live cell imaging to allow for the visualization of possible recruitment or enrichment of MT1-MMP at phagosome associated F-actin foci. The results of this experiment are presented in figure 6.

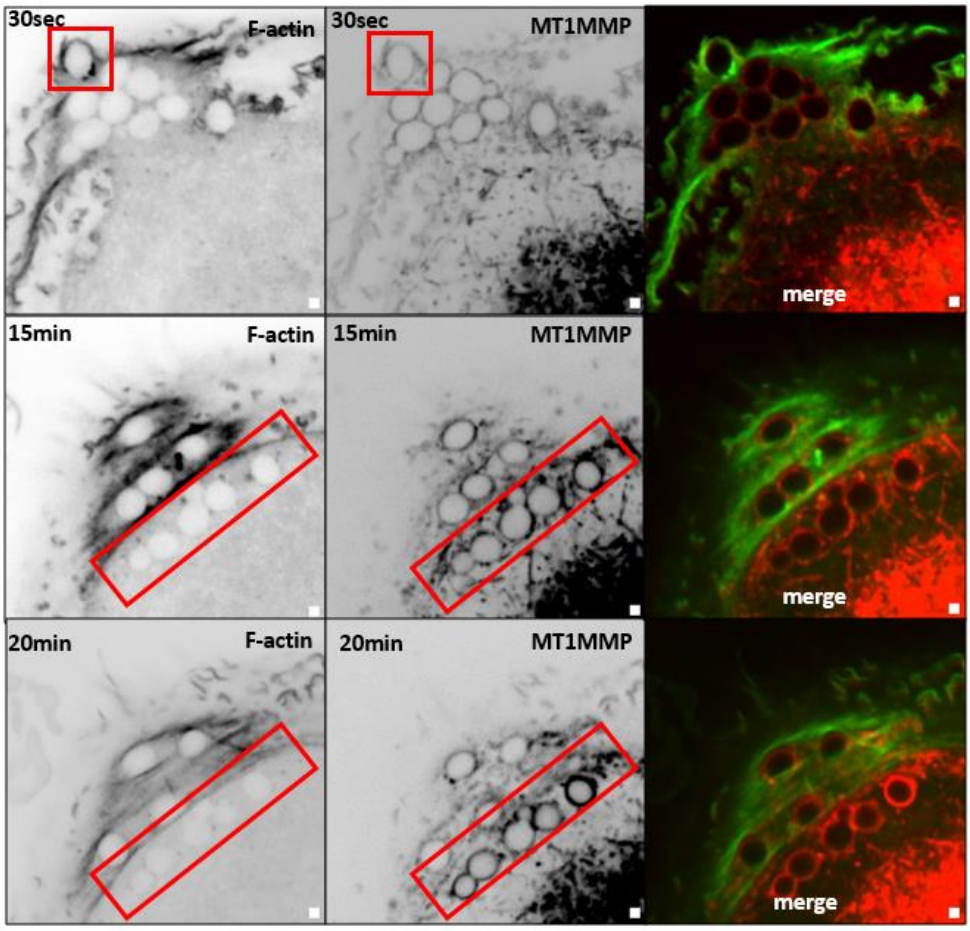

Figure 6: Microscopic images showing the distribution of F-actin Foci (left) and MT1MMP vesicles (right) around candida phagosomes in different stages of phagocytosis in a primary macrophage expressing MT1MMP-mcherry (red) and Lifeact488 (green) construct, with early phagosomes being towards the cell periphery and late phagosomes towards the cell center.

Our results have show that at time 30sec after the uptake of *Candida auris*, F-actin foci start to appear around the phagosomes whereas only few signals of MT1MMP are apparent at this time point. However, as the infection proceeds to 15 min, we notice F-actin foci gradually disappear, while more MT1MMP vesicles appear around the Candida phagosome. 20min through the phagocytic process we notice the complete dissolution of F-actin signals, which is in contrast to very intense MT1MMP signals accumulating all around the phagosomes.

In another experiment concerned with the association of DNase X to phagosomes, specifically in relation to the phagosome–localized F-actin foci, immunofluorescence staining for DNaseX in primary macrophages 20min post infection with *Candida auris* was performed. Respective images presented in figure 7 show that DNaseX signals not only do localize to Candida phagosomes but rather exist in close proximity to F-actin foci.

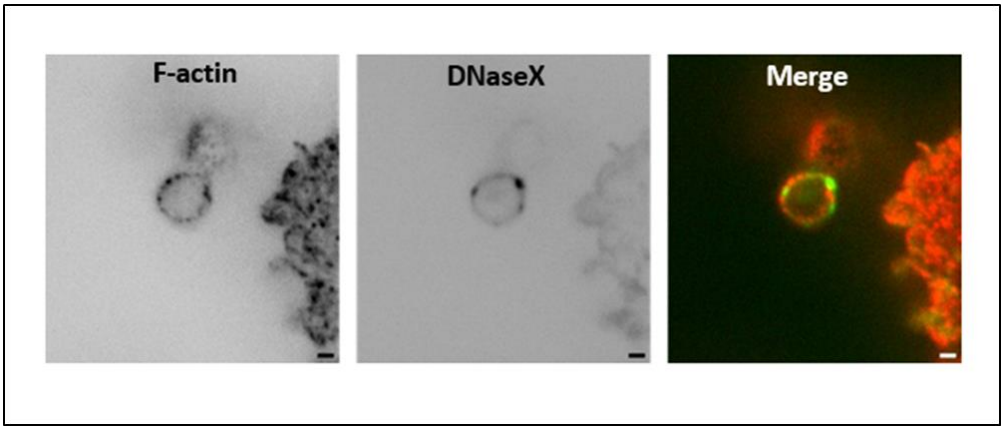

Figure 7: microscopic images from immunofluorescent staining of macrophages for DNaseX using alexa fluor 566 (red)-labeled secondary antibody and phalloidin 488 (green) for F-actin signals, showing the close localization of DNaseX and F-actin foci at Candida phagosome.

3.5 Inhibition of Src tyrosine kinase by PP2

In order to investigate the possible resistance or susceptibility of phagosome specific F-actin foci to specific podosomal protein inhibitors, experiments were conducted with PP2 which is a Src tyrosine kinase inhibitor and DMSO as a control. The appearance of phagosome associated F-actin foci as well as Matrix associated podosomes was then compared and evaluated in both cell poulations at different times after infection (5, 10, 20, 40, 60 min) respectively.

Quantification of matrix associated podosomes per surface area showed statistically significant differences in this matrix associated podosomal abundance between the 2 cell populations that are treated with DMSO and PP2 respectively where the podosomal density ranged between 140 podosomes/1000 μm^2 at 5 min post infection and 160 podosomes/1000um2 at 40 min post infection in cell populations treated with DMSO. However, in the cell population treated with PP2, the number of podosomes per surface area was significantly lower, ranging between 40

podosomes/1000 μm^2 at 40 min post infection and 70 podosomes/1000 μm^2 at 60 min post infection. The corresponding results are presented in Figure 8A.

Upon quantification of podosomes at the level of the formed phagosomes at different times post Candida infection, the cell population treated with DMSO showed statistically significant higher number of phagosomes with podosomes ranging between 45% and 55% phagosomes with podosomes at 10 and 20 min post infection respectively. In contrast to that, the cell population treated with PP2 showed significantly lower values ranging between 23 and 18% at 10 and 20 min after infection respectively. The corresponding results are presented in Figure 8-B.1.

Further analysis of the number of podosomes per phagosomes showed statistically significant higher numbers of podosomes/phagosome at 5, 10 and 20 min after infection, respectively, in cell populations treated with DMSO, with an average ranging between 1.9 and 2.1 at 5min and 10 min post infection respectively compared to cell populations treated with PP2 where the average number of podosomes per phagosome ranged between 0.2 podosomes/phagosome at 20min and 0.5 podosomes/phagosome at 5min post infection. The corresponding results are presented in figure 8B.2.

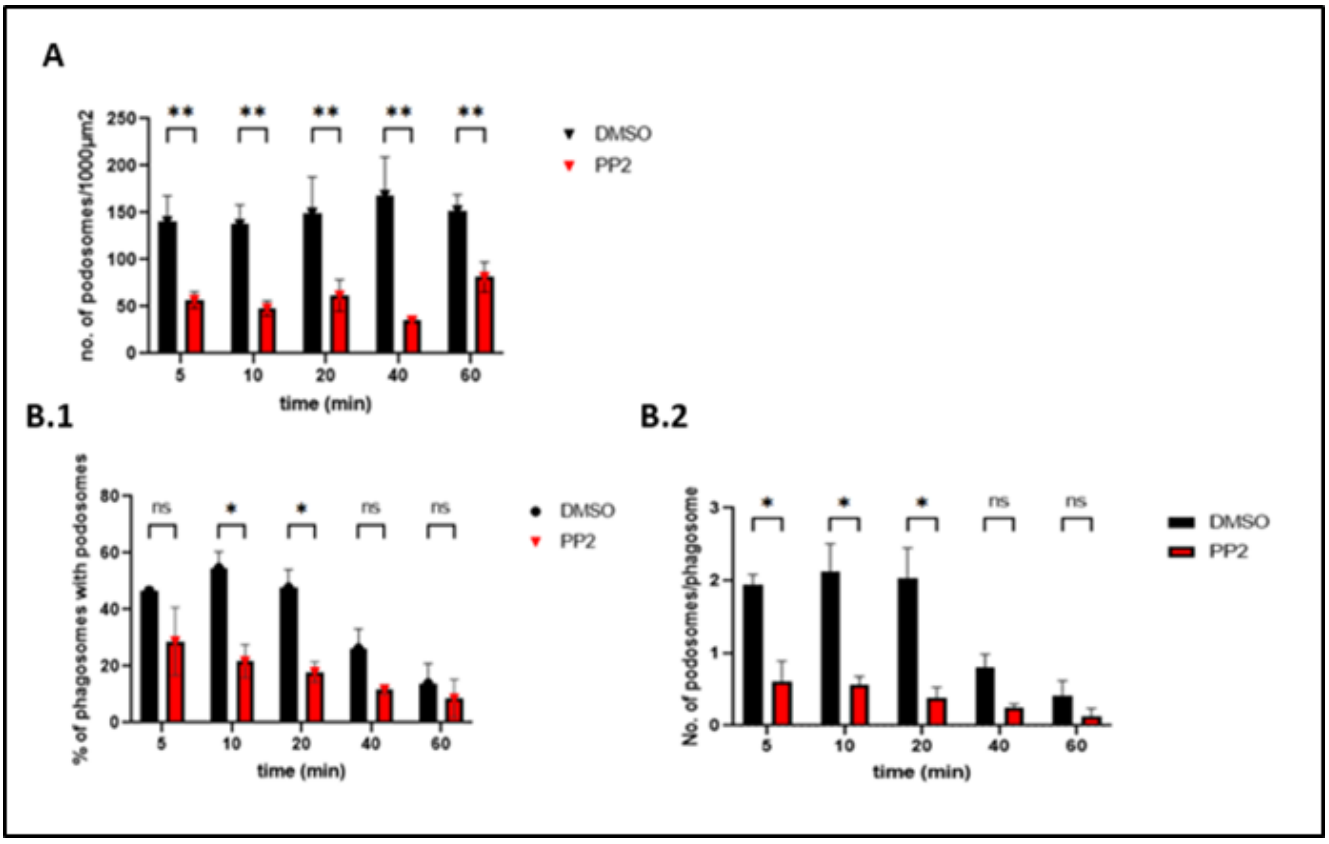

Figure 8: A-a graphic representation of the number of matrix podosomes per surface area (1000um2) at different times post infection as a function of the use of DMSO and PP2 (Tyrosine kinase inhibitor) with data gathered from 3 different donors and analysed using multiple unpaired t-tests with ($P < 0.05$). B.1- a graphic representation showing the variation in % of phagosomes with podosomes at diiferent times post after infection as function of the use of DMSO and PP2(multiple unpaired t-tests, $P < 0.05$). B.2 a graphic representation of the variation in the number of podosomes/phagosome at different times after infection as a function of the use of DMSO and PP2 (multiple unpaired t-tests, $P < 0.05$)

Microscopy images of specimens fixed at 20 min after infection stained for F-actin and PY99 in cell populations treated with DMSO and PP2 showed a clear simultaneous distortion of both F-actin and PY99 podosomal signals. The respective images are presented in figure 9A. on the other hand microscopy images depicting phagocytic podosomes on Candida phagosome at 20 min post infection show more frequent PY99 dot like signals in cell populations treated with DMSO as compared to cell populations treated with PP2. The corresponding images are presented in Figure 9B.

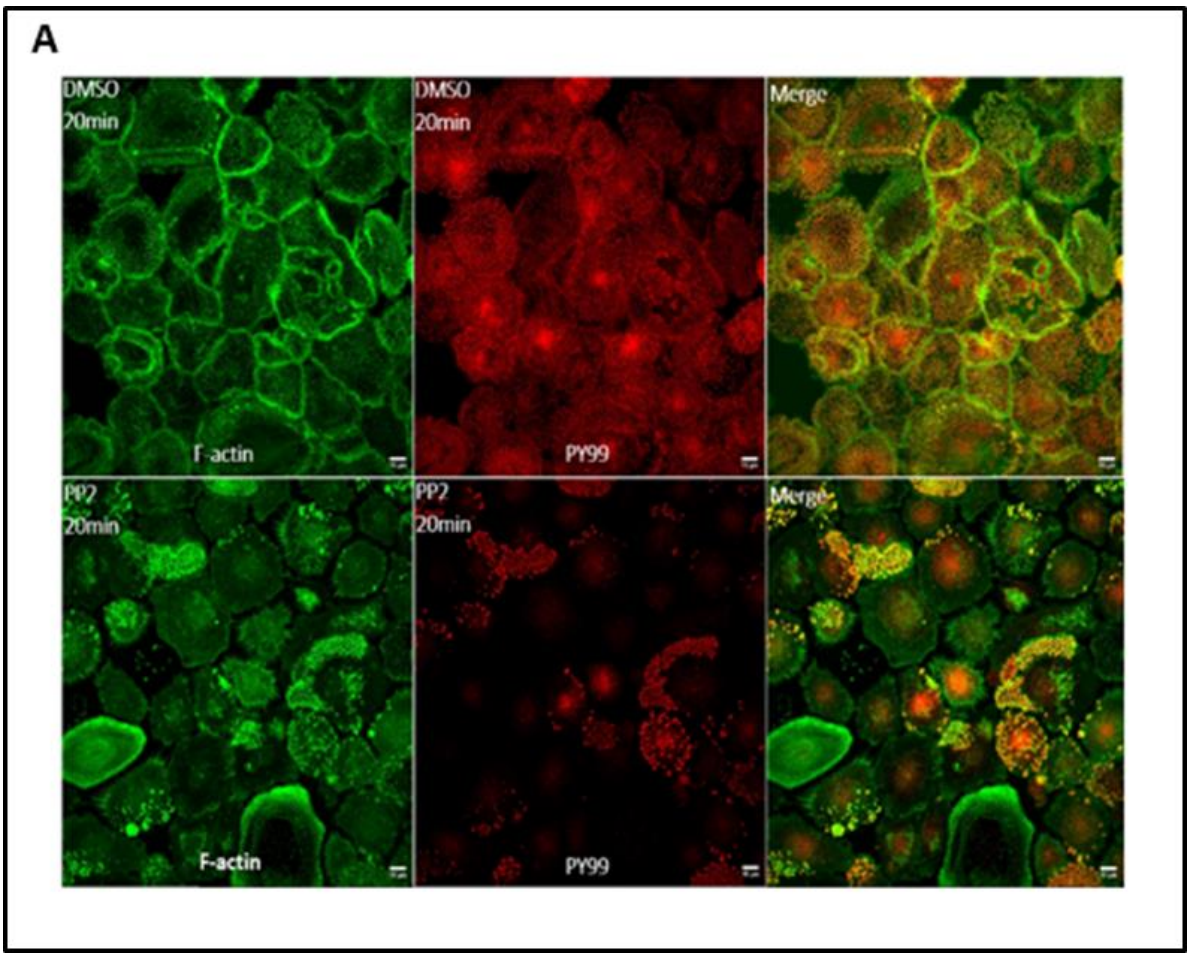
A
DMSO
20min
F-actin
DMSO
20min
PY99
Merge
PP2
20min
F-actin
PP2
20min
PY99
Merge

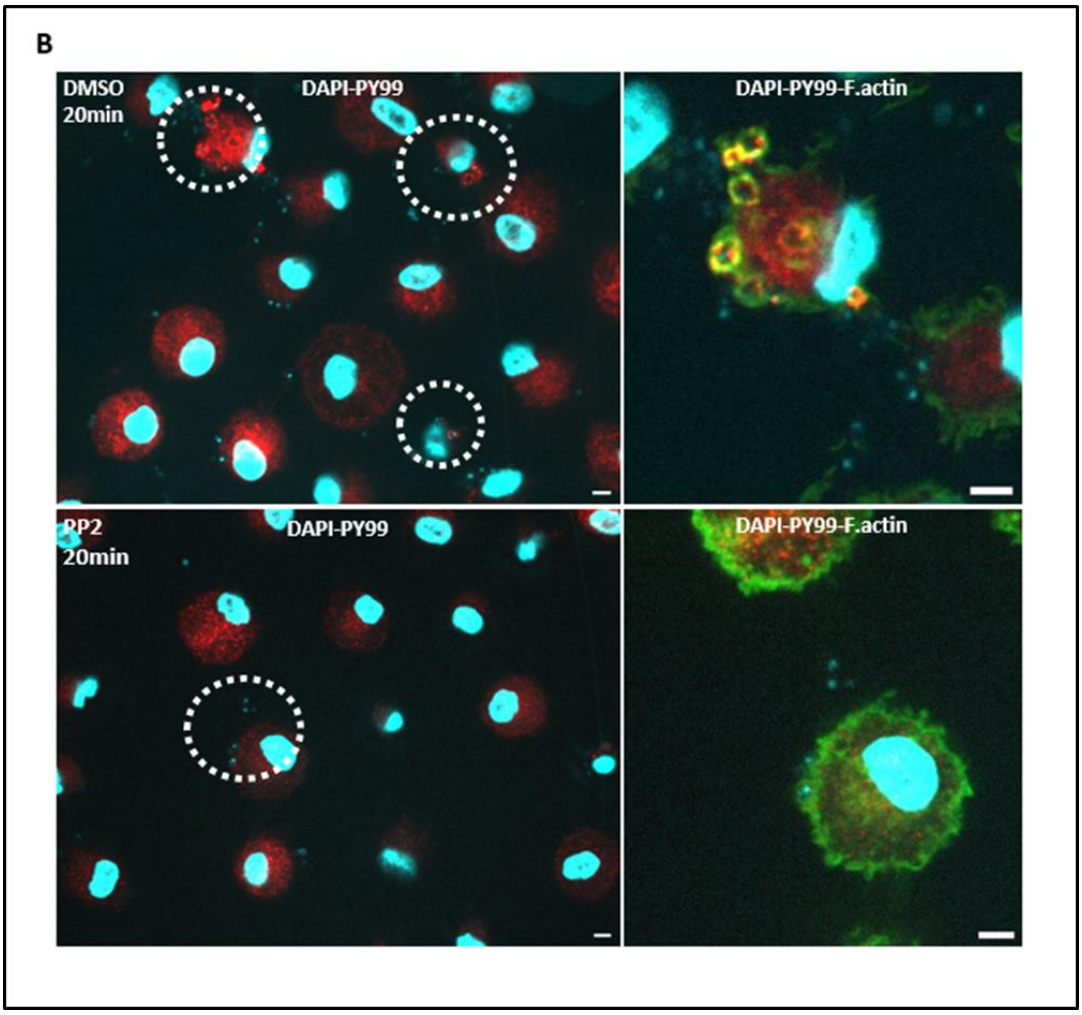

Figure 9: A-Microscopic images of macrophages 20min post infections with *Candida auris,* showing the variation of PY99 red (alexa fluor 566 secondary staining) and F-actin green (Phalloidin 488) signals when in PP2 and DMSO containing mediums respectively. B-microscopic images showing the variation in the number of phagosome associated F-actin foci in 2 primary macrophage populations incubated in PP2 and DMSO containing mediums respectively, where DAPI 405 (cyan) is used to stain for DNA (Candida and macrophage nuclei) and alexa fluor 566 (red) is used as a secondary staining for PY99 and Phalloidin 488 (green) to stain for F-actin. Respective ROI images of both cell populations are added to the right of every image

4-DISCUSSION

4.1 Identification of Podosome-Like Structures on Candida Phagosomes

Phagocytosis is defined as the internalization of particles with a diameter >0.5 μm into phagocytic cells. This process involves actin rearrangements that are crucial for the formation of a phagocytic cup that comprises a homogeneous coat of F-actin that wraps around the ingested particle throughout the whole internalization process and ends up in the formation of closed a phagosome that undergoes further maturation processes leading to particle degradation (Rosales & Uribe-Querol - BioMed Research International – 2017).

In contrast to general assumptions, previous experiments conducted with opsonized latex beads and zymosan have suggested not a continuous, but rather a discontinuous arrangement of F-actin around particles, leading to the formation of distinct F-actin foci around phagosomes that resemble podosomes in terms of size, structure, and composition (Tertrais et al. - European Journal of Cell Biology – 2021).

In this study, we replicate these initial experiments, for the first time with a living biological target particle that we chose to be cells of different *Candida species*, *Candida auris* and *Candida albicans*

Initial fluorescent staining experiments demonstrated the appearance of F-actin foci around phagosomes in a similar manner to what was previously demonstrated with latex beads, indicating that, contrary to the previously described continuous actin rearrangement in phagosomes within the phagocytic cup, the actin reorganizations takes the form of discreet discontinuous foci, consistent with the formation of phagocytic podosomes

4.2 Similar Protein composition of Matrix- associated and phagocytic podosomes

Podosomes consist of > 300 different components that give rise to their full architecture (Weber et al. - European Journal of Cell Biology - 2022). Main substructures include the F-actin-rich core containing branched actin filaments that is surrounded by a discontinuous ring structure consisting of several clusters of adhesion plaque proteins including vinculin, as well as cap structure consisting of actomyosin-regulating proteins such as lymphocyte-specific protein

1 (LSP1) or α-actinin that is localized on top of the core (Weber et al. - European Journal of Cell Biology - 2022).

Following up on the appearance of potential phagocytic podosomes on Candida phagosomes, we conducted immune-staining experiments for a group of proteins that are typical components of core, ring and cap structures of matrix podosomes . These experiments validated the presence of these proteins at the identified actin foci (phagocytic podosomes) as well as their similar localization relative to the actin core as in matrix podosomes Investigated proteins such as cortactin and Arp2 as well as cap proteins such as gelsolin , LSP1 and α-actinin that showed signals that are overlapping with F-actin signals and ring proteins showed a pattern surrounding the F-actin core rather than any overlap.

These findings are in line with previous experiments using opsonised latex beads, especially for the core protein Cortactin and ring protein vinculin (Tertrais et al. - European Journal of Cell Biology – 2021). The results further provide additional information about the presence of podosomal cap structure proteins that are only newly investigated in this study as well as other core and ring proteins in phagocytic podosomes

Despite this growing evidence that these phagosomal structures resemble podosomes in protein composition, further investigations are still needed to locate these proteins in the podosomal microstructure using superresolution microscopy.

Tyrosine kinases were also previously described to have higher activity at the level of matrix associated podosomes especially considering that their activation is associated with the reorganization of actin in specific adhesion structures (Destaing et al. - Molecular Biology of the Cell – 2008). In a previous study, expression of v-Src, the oncogenic form of Src, induces a rearrangement of the actin cytoskeleton characterized by a switch from stress fibers to podosomes in BHK cells (Destaing et al. - Molecular Biology of the Cell – 2008). Hence, these tyrosine kinases enable podosome formation resulting in higher concentrations of phosphorylated tyrosine residues at these areas. Immune-staining results using a phosphotyrosine-specific antibody (PY99) showed dot like foci that are overlapping with the F-actin foci indicating that high density of phosphotyrosine residues, and thus high tyrosine

kinase activity, is present at phagocytic podosomes in a similar manner to matrix associated podosomes.

4.3 Phagocytic podosomes: lifespan and density analysis

Previous studies on the lifespan of matrix associated podosomes showed an average halflife between 2 and 12 minutes, it being dependent on the substrate on which these podosomes are formed (Destaing et al., 2003). These matrix associated podosomes were described as dynamic structrues with a high and fast actin turn over where the F-actin core is replaced from 2 up to 3 times within the lifespan of the individual podosome. Additionally, these matrix podosomes were found to be motile within a certain radius, however, the movement of larger podosome groups is carried out through assembly at the front and disassembly at the rear that is especially visible in migratory cells (Linder & Kopp - Journal of Cell Science – 2005)

In this study, we investigate the lifetime of the identified phagocytic podosomes through live cell imaging techniques and trackmate software analysis. Results showed that the average lifespan of phagocytic podosomes of 1.65 min with a standard deviation of 2.05 min which highlights a main discrepancy of phagocytic podosomes relative to matrix associated podosomes in that they have a significantly shorter lifespan.

Additionally, experiments investigating the lifespan of phagocytic podosomes carried out with opsonized latex beads predicted a lifespan of 5.0 +/- 3.3 min (Tertrais et al. - European Journal of Cell Biology – 2021) which remains significantly lower than those of matrix associated podosomes but different from our obtained results on Candida phagosomes, which brings in again the need to address possible features leading to such a lifespan variation.

Previous studies have shown that the formation of matrix associated podosomes is guided by cues originating from the substratum that cells encounter including composition, density, connectivity, and also topography or roughness of the extracellular matrix (ECM) where podosomes tend to be more stable on rough surfaces and to form preferentially at surface discontinuities. Additionally, Substrate rigidity or stiffness has been identified as a crucial

matrix property that influences podosome formation on a variety of or surfaces (Weber et al. - European Journal of Cell Biology – 2022). It can thus be hypothesized that the variation in podosomal lifespan between our results and previous experiments with either opsonized latex beads or matrix associated podosomes can be explained partially by the different topographical and stiffness characteristics of substrates that phagocytic podosomes are based upon. Additionally, the phagosome on which phagocytic podosomes are based is also a highly dynamic transient structure that undergoes complex modification within a relatively short interval of time leading to particle degradation, which could be an additional factor supporting the reasoning behind the present variations. However, future experiments with particles of different textures and stiffness should provide more accurate information on this point.

The trajectory of phagocytic podosomes could not be thoroughly investigated because the followed trajectory in this study was highly influenced by the phagosomal movement rather than podosomes themselves. However the different trajectory directions of individual podosomes along the same phagosome hint towards the possible motility of these phagocytic podosomes within a certain radius and this is to be further investigated through more complex 3D tracking techniques.

In this study, the presence of podosomes on phagosomes after different times post infection was quantified. The results showed that phagocytic podosomes tend to occur during the early stages of phagocytosis and then disappear as the phagosome undergoes further maturation. Additionally, the average number of podosomes per phagosomes was also higher in early phagosomes than later ones. These findings are in line with experiments designed by Isabelle Maridonneau-Parini, where phagocytic podosomes formed on latex beads tend to start disappearing upon the recruitment of Lamp1 and phagolysomal vesicles later in the phagocytic process (Tertrais et al. - European Journal of Cell Biology – 2021). The exact role of these phagocytic podosomes is yet to be further investigated. However, the timing of their appearance and disappearance suggests a possible role in the initial uptake process, the enclosement of phagosomes and the early phagosomal maturation stages.

4.4. Association of phagocytic podosomes with degradation enzymes

In this study, we investigate the association of phagocytic podosomes with 2 degradative enzymes, DNase X and MT1-MMP, that are known to be associated with matrix associated podosomes to help in the degradation of extracellular matrix or DNA (El Azzouzi et al. - Journal of Cell Biology – 2016), (Pal et al. - Journal of Cell Biology – 2021).

Degradation of the ECM is a key function of podosomes. To achieve this function, podosomes have been shown to recruit matrix-degrading enzymes such as matrix metalloproteinases (Linder et al. - Annual Review of Cell and Developmental Biology - 2011). In this context, membrane-bound metalloproteinase MT1-MMP has emerged as a critical regulator of matrix degradation of podosomes where surface-exposed MT1-MMP at podosomes were detected along with islets that are embedded in the ventral plasma membrane (El Azzouzi et al. - Journal of Cell Biology – 2016).

Our Live-imaging results for cells expressing MT1MMP-mCherry and lifeact-GFP constructs showed that F-actin foci are formed early in the process of internalization with a minimal recruitment of MT1MMP vesicles to phagosomes at this stage, however as the F-actin coat and phagocytic podosomes become more undetectable, the MT1MMP recruitment tends to become more pronounced at the these phagosomes. The exact relationship between these phagocytic podosomes and MT1MMP recruitment to phagosomes remains unclear, however it is possible that these phagocytic podosomes have a role in allowing or blocking the recruitment of MT1MMP vesicles to phagosomes. This would be in line with what is described in the literature about the thinning of the F-actin coat that allows for recruitment of phagolysosomal enzymes to phagosomes such as LAMP1, where the magnitude of the F-actin network surrounding the phagosome has been proposed to preclude association with endocytic organelles (Poirier et al. - Journal of Cell Science – 2020). Additionally, it was also seen that F-actin flashes on phagosomes lead to the deformation of particles leading to their fragmentation and increasing the surface area of the phagosome contents leading to a more efficienct degradation later by proteolytic enzymes after lysosome fusion (Poirier et al. - Journal of Cell Science – 2020) which in its turn can be another link between phagocytic podosome appearance and the delayed MT1MMP recruitment. This hints to possible degradation

pathway that brings enhanced mechanical degradation prior to enzymatic degradation into play.

DNaseX on the other hand is a secretory endonuclease that hydrolyzes DNA to 3'-hydroxyl oligonucleotides in the presence of divalent metal ions, such as Ca^{2+}, Mg^{2+}, and Mn^{2+}. It was demonstrated that DNaseX plays an important role in eliminating extracellular DNA that can cause auto-immune diseases in animals and was later known to be expressed on the cell surface as a glycosylphosphatidylinositol anchored membrane protein (Shiokawa et al. - Journal of Biological Chemistry – 2007). Recent studies revelaed that DNase is consistently and ubiquitously recruited to both matrix associated podosomes and invadopodia. (Pal et al. - Journal of Cell Biology – 2021). In our study, immunostainings of DNaseX showed signals that localize to Candida phagosomes and are in close proximity to phagocytic podosomes as well. Solitary DNase signals on phagosomes, independent of phagocytic podosomes, were also seen. This could indicate that the recruitment of DNaseX can be influenced by phagocytic podosomes in a similar fashion to MT1MMP, however, such hypothesis still needs to be further investigated through analysis of different time points post infection in macrophages expressing DNaseX and lifeact DNA constructs in order to identify the exact sequence of recruitment events. Additionally possible Podosomal pharmacological inhibition experiments and the consequential influence on DNaseX recruitment can also be a useful tool.

4.5. Susceptibilty of phagocytic podosomes to chemical inhibition

The nonreceptor tyrosine kinase Src plays multiple roles in integrin signaling, in the regulation of the cell cytoskeleton and in cell migration (Destaing et al. - Molecular Biology of the Cell – 2008). Furthermore, Src activation is associated with the reorganization of actin in specific adhesion structures. It was found that Expression of v-Src, the oncogenic form of Src, induces a rearrangement of the actin cytoskeleton characterized by a switch from stress fibers to podosomes in BHK cell (Destaing et al. - Molecular Biology of the Cell – 2008). These and other additional roles of tyrosine phosphorylation regulate podosome formation on a fibronectin substrate and actin dynamics within podosomes (Dovas et al. - Journal of Cell Science – 2009).

In this study, and in order to investigate similar possible roles of tyrosine kinases on identified phagocytic podosomes, we chemically inhibited the activity of tyrosine kinases using PP2 in comparison to control cell populations treated with DMSO. Results showed that inhibition of tyrosine kinase activity leads to a significant disruption of both matrix associated podosomes, and also of phagocytic podosomes. This indicates that the regulation and formation of phagocytic podosomes is governed by processes that are tyrosine kinase dependent.

It is also worth mentioning that results show a delay in the inhibition of phagocytic podosome formation compared to matrix associated podosomal inhibition, that we hypothesise is due to the intracellular localisation of phagogocytic podosomes in comparison with the peripheral localization of matrix associated podosomes, close to the cell surface, that could allow the PP2 inhibitor within the culture medium to exert its effect earlier.

The exact protein phosphorylation cascades involved in phagocytic podosomal formation are still not well known, but we would expect a cascade that is quite similar to that involved in matrix associated podosomes, having in mind that there exists room for discrepancies in these cascades between the 2 populations of podosomes. This was demonstrated in experiments conducted on opsonized latex beads where phagocytic podosomes showed partial resistance to chemical inhibition of Arp2/3 complex by CK66, which is in contrast to almost full disruption to matrix associated podosomes by the compound (Tertrais et al. - European Journal of Cell Biology – 2021).

4.6. Conclusion

In conclusion, our study has provided evidence about the occurrence of phagocytic podosomes in the phagocytosis of living biological samples, specifically of cells from different *Candida species*. In contrast, previous studies were all performed with artificial samples, leaving the potential biological relevance of phagocytic podosomes unclear**.**

Furthermore, our results have explored the protein composition of these phagocytic podosomes, and were able to show that phagocytic podosomes contain several typical components of the ring and core structures of matrix-associated podosomes. In addition, we

could also detect proteins of the podosomal cap structures at phagocytic podosomes, although their exact localization within the podosome architecture needs to be further investigated.

Additionally, our study has identified several characteristics of phagocytic podosomes pertaining to their time of appearance and abundance rather early, in the first 20 min of the phagocytic process and their short lifespan of 1,65 +/- 2 min. Moreover, we have also explored the association of these phagocytic podosomes with degradative enzymes in which we were able to hypothesize a possible role for phagocytic podosome appearance in the recruitment of degradative enyzmes to phagosomes. Finally, we were able to investigate the role of tyrosine kinases in phagocytic podosome formation where these were found susceptible to tyrosine kinase inhibition in a similar manner to matrix associated podosomes.

However, it is important to acknowledge the limitations of our study, including Imaging techniques that could be later upgraded to 3D models and super-resolution imaging as well as analytic techniques that are able to study in depth the phagocytic podosome topography for a better designation of each of core, ring and cap structures. Additionally the possible variability in the formation and lifespan of identified phagocytic podosomes needs to be explored in depth especially towards its dependence on engulfed particle characteristics.

Looking ahead, future research should focus on the association of these phagocytic podosomes with particle degradation and their exact role in this process, being it mechanical or enzymatic, additionally, experiments could also investigate the cascades involved in the formation of theses phagocytic podosomes including their dependence on specific known podosomal proteins. Furthermore, association of these podosomes with membrane lipids still remains an interesting aspect to investigate. Addressing these gaps in knowledge will further enhance our understanding of phagocytosis as a cellular process and its possible pathways which can enhance and inform the development of new approaches to handle Candida infections.

In summary, this thesis contributes to the growing body of evidence supporting the involvement of newly identified structures designated as phagocytic podosomes in phagocytosis and paves the way for a progress towards understanding the cues and mechanisms leading to their formation and governing their function.

5-Summary

Candida auris and *Candida albicans* are fungi that pose significant health risks to humans, with *Candida auris* emerging as an increasingly important pathogen. Understanding how immune cells like macrophages internalize and process these *Candida species* at the molecular level is crucial for combating infections caused by these pathogens. Our study reveals that when primary human macrophages engulf *Candida auris* and *Candida albicans* cells, they form dot-like structures rich in F-actin, resembling podosomes, at the phagosomes containing the fungi. We investigated the composition, structure, dynamics, and responsiveness to pharmacological intervention of these structures. Our findings not only shed new light on the mechanism of Candida uptake and cytoskeletal changes upon internalization by immune cells but also highlight Candida species as the first pathophysiologically relevant targets known to induce the formation of phagocytic podosomes.

5-Zusammenfassung

Candida auris und *Candida albicans* sind Pilze, die erhebliche Gesundheitsrisiken für den Menschen darstellen, wobei *Candida auris* zunehmend als bedeutender Krankheitserreger auftritt. Das Verständnis darüber, wie Immunzellen wie Makrophagen diese Candida-Arten auf molekularer Ebene aufnehmen und verarbeiten, ist entscheidend für die Bekämpfung von Infektionen, die durch diese Erreger verursacht werden. Unsere Studie zeigt, dass primäre humane Makrophagen bei der Phagozytose von *Candida auris*- und *Candida albicans*-Zellen punktartige Strukturen bilden, die reich an F-Aktin sind und den Podosomen ähneln. Diese Strukturen befinden sich an den Phagosomen, die die Pilze enthalten. Wir untersuchten die Zusammensetzung, Struktur, Dynamik und die Reaktion dieser Strukturen auf pharmakologische Eingriffe. Unsere Ergebnisse werfen nicht nur neues Licht auf den Mechanismus der Candida-Aufnahme und die zytoskelettalen Veränderungen bei der Internalisierung durch Immunzellen, sondern heben auch hervor, dass Candida-Arten die ersten pathophysiologisch relevanten Ziele sind, die die Bildung phagozytischer Podosomen induzieren.

6. List of abbreviations:

α: alpha

BSA: Bovine serum albumin

°C: degrees Celsius

cm^2 : square centimeter

CO_2 : carbon dioxide

d : day

ddH_2O: double-distilled water

DMSO: Dimethylsulfoxide

EDTA: ethylenediaminetetraacetic acid

ECM: extracellular matrix

γ: gamma

g :gram

GFP: green fluorescent protein

GPI: glycosylphosphatidylinositol

h : hour

H_2O: water

INF-α :interferon alpha

IL :interleukin

KCl :potassium chloride

KH2PO4 :potassium dihydrogen phosphate

LPS : lipopolysaccharide

LSM: lymphocyte separation medium

M-CSF: macrophage colony-stimulating factor

mg: milligram

MgCl2: magnesium chloride

min: minute

ml : milliliter

mm : millimeter

mM : millimole

MMP : matrix metalloproteinase

mRNA : messenger RNA

MT1-MMP: membrane type 1-matrix metalloproteinase

MΦ :macrophage

nm :nanometer

NaCl: sodium chloride

Na_2HPO_4 : disodium hydrogen phosphate

NaOH: sodium hydroxide

n.s. :not significant

PBS: phosphate-buffered saline

PP2 :PP2 is a reversible and ATP-competitive Src family kinases inhibitor

ROS :reactive oxygen species

rpm :revolutions per minute

RPMI :Roswell Park Memorial Institute (cell culture medium)

SDS :sodium dodecyl sulfate

TGF-β :transforming growth factor-beta

TNF-α :tumor necrosis factor-alpha

µ :micro

µl :microliter

U :unit

UKE :University Medical Center Hamburg-Eppendorf

UV :ultraviolet

VEGF :vascular endothelial growth factor

% : percent

7. BIBLIOGRAPHY

Carlos Rosales, Eileen Uribe-Querol, "Phagocytosis: A Fundamental Process in Immunity", BioMed Research International, vol. 2017, Article ID 9042851, 18 pages, 2017. https://doi.org/10.1155/2017/9042851

Jaumouillé, V., & Waterman, C. M. (2020). Physical Constraints and forces involved in phagocytosis. Frontiers in Immunology, 11. https://doi.org/10.3389/fimmu.2020.01097

Uribe-Querol, E., & Rosales, C. (2020). Phagocytosis: Our current understanding of a universal biological process. Frontiers in Immunology, 11. https://doi.org/10.3389/fimmu.2020.01066

Van Goethem, E., Guiet, R., Balor, S., Charrière, G. M., Poincloux, R., Labrousse, A., Maridonneau-Parini, I., & Le Cabec, V. (2011). Macrophage podosomes go 3D. European Journal of Cell Biology, 90(2–3), 224–236. https://doi.org/10.1016/j.ejcb.2010.07.011

Stefan Linder, Petra Kopp; Podosomes at a glance. J Cell Sci 15 May 2005; 118 (10): 2079–2082. doi: https://doi.org/10.1242/jcs.02390

Linder, S., & Barcelona, B. (2023). Get A grip: Podosomes as potential players in phagocytosis. European Journal of Cell Biology, 102(4), 151356. https://doi.org/10.1016/j.ejcb.2023.151356

Italiani, P., & Boraschi, D. (2014). From monocytes to M1/M2 macrophages: Phenotypical vs. functional differentiation. Frontiers in Immunology, 5. https://doi.org/10.3389/fimmu.2014.00514

Schachtner, H., Calaminus, S. D., Thomas, S. G., & Machesky, L. M. (2013). Podosomes in adhesion, migration, Mechanosensing and matrix remodeling. Cytoskeleton, 70(10), 572–589. https://doi.org/10.1002/cm.21119

Linder, S., & Kopp, P. (2005). Podosomes at a glance. Journal of Cell Science, 118(10), 2079–2082. https://doi.org/10.1242/jcs.02390

Yunna, C., Mengru, H., Lei, W., & Weidong, C. (2020). Macrophage M1/M2 polarization. European Journal of Pharmacology, 877, 173090. https://doi.org/10.1016/j.ejphar.2020.173090

Aldejohann, A. M., Martin, R., Hecht, J., Haller, S., Rickerts, V., Walther, G., Eckmanns, T., & Kurzai, O. (2023). Rise in candida auris cases and first nosocomial transmissions in Germany. Deutsches Ärzteblatt International. https://doi.org/10.3238/arztebl.m2023.0047

Sato, M. C. (2023). Candida auris: a novel emerging nosocomial pathogen – properties, epidemiological situation and infection control. GMS Hygiene and Infection Control. https://doi.org/10.3205/dgkh000444

Ana Pérez, Gordon Ramage, Rosario Blanes, Amelia Murgui, Manuel Casanova, José P. Martínez, Some biological features of Candida albicans mutants for genes coding fungal proteins containing the CFEM domain, FEMS Yeast Research, Volume 11, Issue 3, May 2011, Pages 273–284, https://doi.org/10.1111/j.1567-1364.2010.00714.x

Kabir MA, Hussain MA, Ahmad Z. Candida albicans: A Model Organism for Studying Fungal Pathogens. ISRN Microbiol. 2012 Sep 29;2012:538694. doi: 10.5402/2012/538694. PMID: 23762753; PMCID: PMC3671685.

Chen H, Zhou X, Ren B, Cheng L. The regulation of hyphae growth in Candida albicans. Virulence. 2020 Dec;11(1):337-348. doi: 10.1080/21505594.2020.1748930. PMID: 32274962; PMCID: PMC7161696.

Cottier, F., & Hall, R. A. (2020). Face/off: The interchangeable side of candida albicans. Frontiers in Cellular and Infection Microbiology, 9. https://doi.org/10.3389/fcimb.2019.00471

Wang, Q., Cheng, S., Wang, Y., Li, F., Chen, J., Du, W., Kang, H., & Wang, Z. (2023). Global characteristics and trends in research on candida auris. Frontiers in Microbiology, 14. https://doi.org/10.3389/fmicb.2023.1287003

Kourkoumpetis, T. K., Velmahos, G. C., Ziakas, P. D., Tampakakis, E., Manolakaki, D., Coleman, J. J., & Mylonakis, E. (2010). The effect of cumulative length of hospital stay on the antifungal resistance of candida strains isolated from critically ill surgical patients. Mycopathologia, 171(2), 85–91. https://doi.org/10.1007/s11046-010-9369-3

Brandt, M. E., & Lockhart, S. R. (2012). Recent taxonomic developments with candida and other opportunistic yeasts. Current Fungal Infection Reports, 6(3), 170–177. https://doi.org/10.1007/s12281-012-0094-x

Tertrais, M., Bigot, C., Martin, E., Poincloux, R., Labrousse, A., & Maridonneau-Parini, I. (2021). Phagocytosis is coupled to the formation of phagosome-associated podosomes and a transient disruption of podosomes in human macrophages. European Journal of Cell Biology, 100(4), 151161. https://doi.org/10.1016/j.ejcb.2021.151161

Nguyen, J. A., & Yates, R. M. (2021). Better together: Current insights into phagosome-lysosome fusion. Frontiers in Immunology, 12. https://doi.org/10.3389/fimmu.2021.636078

Krendel, M., & Gauthier, N. C. (2022). Building the phagocytic cup on an actin scaffold. Current Opinion in Cell Biology, 77, 102112. https://doi.org/10.1016/j.ceb.2022.102112

Linder, S., & Kopp, P. (2005). Podosomes at a glance. Journal of Cell Science, 118(10), 2079–2082. https://doi.org/10.1242/jcs.02390

Dovas, A., Gevrey, J.-C., Grossi, A., Park, H., Abou-Kheir, W., & Cox, D. (2009). Regulation of podosome dynamics by wasp phosphorylation: Implication in matrix degradation and chemotaxis in macrophages. Journal of Cell Science, 122(21), 3873–3882. https://doi.org/10.1242/jcs.051755

Destaing, O., Sanjay, A., Itzstein, C., Horne, W. C., Toomre, D., De Camilli, P., & Baron, R. (2008). The tyrosine kinase activity of c-src regulates actin dynamics and organization of Podosomes in osteoclasts. Molecular Biology of the Cell, 19(1), 394–404. https://doi.org/10.1091/mbc.e07-03-0227

Pal, K., Zhao, Y., Wang, Y., & Wang, X. (2021). Ubiquitous membrane-bound DNase activity in podosomes and invadopodia. Journal of Cell Biology, 220(7). https://doi.org/10.1083/jcb.202008079

Shiokawa, D., Matsushita, T., Shika, Y., Shimizu, M., Maeda, M., & Tanuma, S. (2007). DNase x is a glycosylphosphatidylinositol-anchored membrane enzyme that provides a barrier to

endocytosis-mediated transfer of a foreign gene. Journal of Biological Chemistry, 282(23), 17132–17140. https://doi.org/10.1074/jbc.m610428200

Linder, S., Wiesner, C., & Himmel, M. (2011). Degrading devices: Invadosomes in proteolytic cell invasion. Annual Review of Cell and Developmental Biology, 27(1), 185–211. https://doi.org/10.1146/annurev-cellbio-092910-154216

El Azzouzi, K., Wiesner, C., & Linder, S. (2016). Metalloproteinase MT1-MMP islets act as memory devices for podosome reemergence. Journal of Cell Biology, 213(1), 109–125. https://doi.org/10.1083/jcb.201510043

Poirier, M. B., Fiorino, C., Rajasekar, T. K., & Harrison, R. E. (2020). F-actin flashes on phagosomes mechanically deform contents for efficient digestion in macrophages. Journal of Cell Science. https://doi.org/10.1242/jcs.239384

Destaing, O., Saltel, F., Géminard, J.-C., Jurdic, P., & Bard, F. (2003). Podosomes display actin turnover and dynamic self-organization in osteoclasts expressing actin-green fluorescent protein. Molecular Biology of the Cell, 14(2), 407–416. https://doi.org/10.1091/mbc.e02-07-0389

Linder, S., & Aepfelbacher, M. (2003). Podosomes: Adhesion hot-spots of invasive cells. Trends in Cell Biology, 13(7), 376–385. https://doi.org/10.1016/s0962-8924(03)00128-4

Tarone G, Cirillo D, Giancotti FG, Comoglio PM, Marchisio PC. Rous sarcoma virus-transformed fibroblasts adhere primarily at discrete protrusions of the ventral membrane called podosomes. Exp Cell Res. 1985 Jul;159(1):141-57. doi: 10.1016/s0014-4827(85)80044-6. PMID: 2411576.

Burns, S., Thrasher, A. J., Blundell, M. P., Machesky, L., & Jones, G. E. (2001). Configuration of human dendritic cell cytoskeleton by Rho GTPases, the was protein, and differentiation. *Blood*, *98*(4), 1142–1149. https://doi.org/10.1182/blood.v98.4.1142

Seano, G., Daubon, T., Génot, E., & Primo, L. (2014). Podosomes as novel players in Endothelial Biology. European Journal of Cell Biology, 93(10–12), 405–412. https://doi.org/10.1016/j.ejcb.2014.07.009

Burgstaller G, Gimona M. Podosome-mediated matrix resorption and cell motility in vascular smooth muscle cells. Am J Physiol Heart Circ Physiol. 2005 Jun;288(6):H3001-5. doi: 10.1152/ajpheart.01002.2004. Epub 2005 Feb 4. PMID: 15695563.

Daan Vorselen, Sarah R Barger, Yifan Wang, Wei Cai, Julie A Theriot, Nils C Gauthier, Mira Krendel (2021) Phagocytic 'teeth' and myosin-II 'jaw' power target constriction during phagocytosis eLife 10:e6862. https://doi.org/

Allen LA, Aderem A. Molecular definition of distinct cytoskeletal structures involved in complement- and Fc receptor-mediated phagocytosis in macrophages. J Exp Med. 1996 Aug 1;184(2):627-37. doi: 10.1084/jem.184.2.627. PMID: 8760816; PMCID: PMC2192718.

Calderone, R., & Clancy, C. (2012). *Candida and candidiasis*. ASM Press.

Caliman Sato, M, Izu Nakamura Pietro, EC, Marques da Costa Alves, L, Kramer, A, & da Silva Santos, PS. (2023). Candida auris: A novel emerging nosocomial pathogen - properties, epidemiological situation and Infection Control. German Medical Science GMS Publishing House; Düsseldorf.

Buccione R, Orth JD, McNiven MA. Foot and mouth: podosomes, invadopodia and circular dorsal ruffles. Nat Rev Mol Cell Biol. 2004 Aug;5(8):647-57. doi: 10.1038/nrm1436. PMID: 15366708.

8. Acknowledgement

My work throughout this project is dedicated to all the supportive individuals who made this thesis possible.

First and foremost, I express my heartfelt gratitude to my PI, Prof. Dr. Stefan Linder, for providing me with this great research opportunity and his invaluable advice, close monitoring, and guidance throughout all the experiments.

I am also grateful to our Lab MTA, Andrea Mordhorst, for preparing all the necessary experimental reagents and sharing her practical expertise with me, in addition to her pleasant and unique touch and attitude in the entire laboratory environment.

Special thanks to Dr. Pasquale Cervero for assisting in optimizing my practical techniques, providing valuable insights into experimental designs, and offering important advice during data analysis.

I extend my appreciation to all my lab colleagues, Sven Hey, Bryan Barcelona, Marie Vollmost, Themis Paraschiakos , Kathrin Weber, Robert Herzog, and Lars Wiltfang, for their support and for fostering a friendly and conducive laboratory environment.

A heartfelt thank you goes to my colleague, Konstantin Sopelniak, for not only sharing his practical expertise but also for his continuous support during experiments, microscopy, and analysis, as well as for making the laboratory experience enjoyable and fun.

Thanks shall also be extended to the RTG program in which I was a part, and all the administrators working to make it a success, especially Prof. Martin Aepfelbacher for his efforts in this program and the financial support provided. Not to mention all the people at the UKE microscopy facility who assisted in mastering all needed microscopy techniques.

Lastly, I dedicate this work to my home country Lebanon and to my family and friends back there who have always been there to support me, celebrate my achievements and keep pushing me forward.

9. Curriculum vitea

Personal information:

Name: Rawan Batlouni

Nationality: Lebanese

Date of Birth: 01-01-1998

Place of Birth: Baakline, Lebanon

Address: Rawan Batlouni c/o Da Costa Lima,
Billstraße 50, 20539
Hamburg, Germany

Education:

2000-2015

Primary School: Lycee National Schools, Bakaata, Lebanon

Secondary School: Lycee National Schools, Bakaata, Lebanon

Lebanese Baccalaureate

2015-2018

Bachelor of Biological Sciences (Pre-Medical): American University of Beirut, Beirut, Lebanon

2018-2022

Doctor of Medicine (MD): University of Balamand, Beirut, Lebanon
Lebanese Medical License

2023-2024

Medical Doctorate (Promotion): University Medical Center Hamburg-Eppendorf,
University of Hamburg, Germany

PROFESSIONAL EXPERIENCE

Intern, University Medical Center Hamburg-Eppendorf (UKE) - Department of General Visceral and Thoracic Surgery (01-02-2024 to 30-03-2024)

Medical Student Intern, St. Elisabeth Hospital, Neuburg an der Donau, Germany (02-04-2022 to 01-05-2022)

Medical Student Intern, St. Joseph Hospital, Freiburg, Germany (01-03-2022 to 01-04-2022)

Medical Student Intern, Saint Georges University Hospital, Beirut, Lebanon (01.07.2020 to 01.06.2022)

Medical Student Intern, Mount Lebanon Hospital, Beirut, Lebanon (01.07.2020 to 01.06.2022)

Medical Student Intern, Uniwersytecki Szpital Kliniczny im.N. Barlickiego w Lodzi, Lodz - Poland. (01.06.2019 to 01.07.2019)

Memberships:

Lebanese Red Cross –Youth: General member (01.06.2015 – 01.06.2017) Baakline, Lebanon.

AUB outlook Student newspaper: Editor in Chief (01.02.17 – 01.02.18) Beirut, Lebanon.

Languages:

Arabic: Native

English: Excellent

German: Proficiency level C1

French: Proficiency level A2

10. Eidesstattliche Versicherung

Ich versichere ausdrücklich, dass ich die Arbeit selbständig und ohne fremde Hilfe verfasst, andere als die von mir angegebenen Quellen und Hilfsmittel nicht benutzt und die aus den benutzten Werken wörtlich oder inhaltlich entnommenen Stellen einzeln nach Ausgabe (Auflage und Jahr des Erscheinens), Band und Seite des benutzten Werkes kenntlich gemacht habe.

Ferner versichere ich, dass ich die Dissertation bisher nicht einem Fachvertreter an einer anderen Hochschule zur Überprüfung vorgelegt oder mich anderweitig um Zulassung zur Promotion beworben habe.

Ich erkläre mich einverstanden, dass meine Dissertation vom Dekanat der Medizinischen Fakultät mit einer gängigen Software zur Erkennung von Plagiaten überprüft werden kann.

Unterschrift: